2019

# CLOSED LOOP ENERGY MAXIMIZING CONTROL OF A WAVE ENERGY CONVERTER USING AN ESTIMATED LINEAR MODEL THAT APPROXIMATES THE NONLINEAR FROUDE-KRYLOV FORCE

Yaqzan Mohd Yaqzan
*Michigan Technological University*, myaqzan@mtu.edu

# CLOSED LOOP ENERGY MAXIMIZING CONTROL OF A WAVE ENERGY CONVERTER USING AN ESTIMATED LINEAR MODEL THAT APPROXIMATES THE NONLINEAR FROUDE-KRYLOV FORCE

By

Mohd Yaqzan

A THESIS

Submitted in partial fulfillment of the requirements for the degree of

MASTER OF SCIENCE

In Mechanical Engineering

MICHIGAN TECHNOLOGICAL UNIVERSITY

2019

This thesis has been approved in partial fulfillment of the requirements for the Degree of MASTER OF SCIENCE in Mechanical Engineering.

Department of Mechanical Engineering-Engineering Mechanics

Thesis Advisor: *Dr. Gordon G. Parker*

Committee Member: *Dr. Wayne W. Weaver*

Committee Member: *Dr. Jason R. Blough*

Department Chair: *Dr. William W. Predebon*

# Contents

# List of Figures

# List of Tables

# Acknowledgments

In the name of God, Most Gracious, Most Merciful.

*"Read! And your Lord is the Most Generous, Who has taught (the writing) by the pen, Has taught man that which he knew not."* (96:3-5)

---

First and foremost, I wish to express my deepest appreciation to my adviser, Prof. Dr. *Gordon G. Parker* for his enthusiasm, constant encouragement and able supervision. Gordon inspired me through his teaching and sparked the engineer inside me long before I decided to pursue research under his guidance. I sincerely thank him for giving me a research topic. His vast knowledge over the subject and broadly in the dynamics field guided me to remove many misconceptions, helped me to broaden my own understanding and made me love the process even more. I'd still probably be trying to get my model running on a computer if it weren't for him. Those uncountable hours of long discussion are highly appreciated. Innumerable times he helped to point me in the right direction.

I would also like to give thanks and appreciation to my fellow members of the Intelligent Systems and Controls Lab. I, of course, consider them all to be my colleagues, but I also consider them to be my friends. *Eddy Trinklein, Sal Husain, Robert Jane* and *Sam Swartzmiller* gave valuable one-on-one time allowing me to keep the research on track. Special thanks to *Sal Husain* who provided some of his models and data to support this work. Also, a big thanks to *Emma Lozon* for proofreading and providing constructive feedback on my thesis.

Thanks goes to the other members of the dissertation committee: *Wayne W. Weaver* and *Jason R. Blough*. Thank you for taking the time to provide feedback on this thesis and your willingness work with a less than typical schedule.

It is an immense pleasure to express my gratitude and deep love to my mother and father, who over last two decades, together bore all the hardships of life. Their each and every step, explicitly or implicitly, was for my success. Words are so insufficient to quantify sacrifices made by them. Last but not least, I thank *Mariya* for her love and support. Without her, it would have been very difficult to stay focused.

This thesis is dedicated to all of you.

# List of Abbreviations

| | |
|---|---|
| ANN | Artificial Neural Network |
| AWS | Archimedes' Wave Swing |
| BEM | Boundary Element Method |
| BES | Battery Energy Storage |
| CCC | Complex Conjugate Control |
| CFD | Computational Fluid Dynamics |
| DP | Dynamic Programming |
| FRC | Force Control |
| GPS | Global Positioning System |
| IRF | Impulse Response Function |
| LQ | Linear Quadratic |
| MPC | Model Predictive Control |
| OWC | Oscillating Water Column |
| PAD | Percentage Amplitude Difference |
| PD | Proportional Derivative |
| PTO | Power Take Off |
| QP | Quadratic Programming |
| SDOF | Single Degree of Freedom |

| | |
|---|---|
| SWL | Stationary Water Level |
| SB | Shape Based |
| WEC | Wave Energy Converter |

# Abstract

Wave energy converters (WECs) exploit ocean wave energy and convert it into useful forms such as electricity. But for WECs to be successful on a large scale, two primary conditions need to be satisfied. The energy generated must satisfy the network requirements, and second, energy flow from waves to the grid needs to be maximized. In this dissertation, we address the second problem. Most control techniques for WECs today use the Cummins' linear model to simulate WEC hydrodynamics. However, it has been shown that under the application of a control force, where WEC motions are amplified, the linear model diverges from actual motions. Hence, it becomes necessary to model the nonlinear motion for realistic energy capture prediction. In this work, it is shown that a closed form energy optimal solution to the nonlinear model requires satisfaction of initial conditions that violate physical restrictions. Numerical optimization based controllers that use physical constraints as a necessary condition require large computation costs and are difficult to implement in real time. To mitigate computation costs for real-time implementation while precisely predicting nonlinear behavior, an efficient method of modelling WECs using an estimated linear model for computing the energy optimal control solution is presented. The estimated linear model is compared against the Cummins' model for accuracy of motion during an uncontrolled case. It is also shown that, there exists a force which results in higher energy extraction than optimal force from Cummins' model when applied to a

nonlinear model. Additional analyses are also performed to evaluate the robustness of the proposed method in random and extreme sea states.

# Chapter 1

# INTRODUCTION

Global population is continuously increasing and more and more resources are being used on a daily basis. Although fossil fuels have been the major sources of energy, the need for a sustainable, infinite and clean source of energy is ubiquitous. Environmental problems resulting from fossil fuels such as pollution and greenhouse gas emissions have a negative impact on the climate and human habitation [1]. Renewable sources such as wave energy along with solar, wind, geothermal, etc. can significantly reduce our dependence on fossil fuels due to their enormous abundance. A total of 2.7 - 3 TW of ocean power resources have been estimated worldwide [2]. Mark et al. presents a detailed report on world-wide wave energy potential [3]. Due to this prolific reserve of energy, numerous scientists have tried to convert wave energy into usable forms. It has been reported that inventors registered more than 1000 patents in this field by

1980 [4].

A tremendous amount of ocean wave literature and technology have been extensively theorized over the last three decades. However, in reality, it is very challenging to describe, predict and reproduce conditions at offshore locations for testing purposes. This is because of the complex and innumerable environmental parameters that have significant effect on wave profiles. Spectral representation of ocean waves and their characterization are detailed in [5]. The power produced as a result of reciprocating movement induced by ocean waves is more uneven than other renewable sources. Wave energy converters (WECs) exploit ocean wave energy and convert it into a useful form such as electricity. But for WECs to be successful on a large scale, two primary conditions need to be satisfied. The energy generated must satisfy the network requirements, and second, energy flow from waves to the grid needs to be maximized.

## 1.1 Problem Statement

Some of the earliest work in wave power devices is credited to Girard [6], who experimented with heaving floats in 1799. The most commonly used equation of motion to model WECs was derived by Cummins [7]. Since then, there have been constant

efforts to formulate control strategies for WECs for maximum energy harvesting. Because of the linear nature of this model, well established control methods, (namely, Resistive, Model Predictive Control (MPC), Dynamic Programming (DP), Shape Based (SB) Control, Linear Quadratic (LQ) Control, Latching, etc.) [8] were used by researchers all over the world. Most of the studies rely on major simplifications and assumptions such as accurate incoming wave prediction, Single Degree of Freedom (SDOF) motion, linear or perfectly known non-linear hydrodynamics, no instrument noise, unlimited Power Take-Off (PTO) performance.

Recently, there has been an increase in using nonlinear models to describe WEC dynamics as they are accurate in predicting buoy motion and do not have the limitation of small WEC displacement about the equilibrium position [9]. Moreover, in a quest to implement optimal control, whether using linear or nonlinear models, the relationship of WEC initial displacement and velocity on extracted energy is overlooked.

## 1.2 Aim and Scope

There is a trade-off between WEC model complexity, computation cost and amount of energy extraction. A linear, SDOF WEC model has a well defined closed form optimal control force solution. Whereas, nonlinear models depend upon numerical optimization based controllers that require wave forecasting [10] and hence are often

sub-optimal. Such optimization based controllers are difficult to implement in real-time due to their computational cost. Additionally, optimal solution of such problems requires satisfaction of additional necessary conditions at the beginning or end of the optimal path. The solution to such conditions result in unrealizable motions in the real world [11].

While a linear model has a convenient energy optimal control solution, it is based on the assumption of small WEC displacements about a mean position. This is however not true in reality as the objective of PTO is to enhance those motions. The aim of this thesis is to propose an efficient method of modelling and control of WECs using an estimated form of a nonlinear model. This linear model changes model parameters in real-time to accurately follow the WEC's nonlinear response, thereby making it possible to implement an optimal control force with necessary initial conditions. Due to the continuous parameter update capability of the proposed technique, this method is also robust to drift in WEC parameters over time.

## 1.3 Significance of Study

The proposed method is computationally fast like a linear model but offers the advantage of realizing the effect of nonlinearities induced as a result of a continuously

varying wetted area of buoy. Moreover, with the help of this study, realistic estimates of extracted energy are possible. These estimates are critical in determining the size and shape of individual buoys and arrays in a wave energy farm. The study presented here considers regular waves using optimal control techniques to characterize the effectiveness of the proposed methodology by comparing extracted energy over a definite span of time. Additional analyses are also performed to evaluate the robustness of the proposed method in random and extreme sea states.

## 1.4 Overview

This thesis consists of six chapters within two main parts. Part I comprising chapters 2 and 3, discusses the theoretical groundwork of wave energy conversion terminology, components and control necessary to guide the research. Chapter 2 includes an introduction to ocean waves, types of buoys, converters and PTO units to better understand the dynamics behind their operation. Based on this knowledge, Chapter 3 investigates recent trends and policies in practice today pertaining to wave energy control. It includes a critical review of historical and current practices, identifying pressing areas that require deeper investigation. At this time, an approach to include nonlinear behavior while maintaining ease of control is proposed. In part II, Chapter 4 discusses individual hydrodynamic effects along with their mathematical models. These effects are eventually combined to form a governing equation used for creating

the energy optimal solution. Assumptions are laid down that distinguish a linear and nonlinear model. Chapter 5 goes in detail of the proposed technique, design of experiment, methodology and necessary criteria for success. Derivation of the general form of the energy optimal force for the nonlinear model and its limitations are also presented. Finally, results and conclusions are presented in Chapter 6 with verification of satisfaction of necessary criteria for success with suggestions for future work.

# Chapter 2

# BACKGROUND

This chapter reviews types of waves, WECs and their interaction particularly in heave motion. This chapter forms the basis of understanding how waves are characterized, the wave energy conversion processes and the objective of control strategies for maximum energy extraction.

## 2.1 Ocean Wave Theory

Ocean waves are carriers of energy from one place to another. These waves can be categorized as shallow and deep water waves based upon the ratio of depth of water and wavelength [12]. If this ratio is less than 0.5, we have shallow water waves or

long waves; otherwise if the ratio is greater than 0.5, they are known as deep water waves or short waves. Ocean waves can be produced by meteorological forces such as wind and air pressure as well as astronomical forces like tides and earthquakes resulting in tsunamis. In short waves, the rate of energy dissipation of waves is much smaller compared to the wind from which they originate. This enables these waves to last longer than the wind [13]. This phenomenon happens over large regions that ultimately results in storage and concentration of useful energy both temporally and spatially in these waves. Energy concentration is directly proportional to the density of the medium. This results in more concentration of energy delivered by waves as their density is 3 orders of magnitude higher than wind.

On a simplistic level, an ocean wave can be thought of as a sinusoidally travelling disturbance with crests and troughs in a definite direction. According to this model, as the water surface oscillates up and down, there is a circular motion of water particles about the mean central position. This central line remains unchanged in time and serves as a baseline for measuring WEC motions. Due to the relation between the motion of water particles and the water surface, the amplitude and frequency of a wave can be described in terms of its particle's motion. As a result, the amplitude of a wave is the radius of circular motion of particles whereas, the frequency equals the angular velocity. On the same lines, the rate of change of wave elevation with respect to time is equal to the vertical velocity of individual particles on the surface. However, this model, like any mathematical model, is based on some assumptions. It

is valid only when the effect of viscosity on the motion of particles is neglected and the fluid is assumed to be in-compressible.

### 2.1.1 Linear and Nonlinear Waves

As already stated, waves can be described as sinusoidal variations at the water surface and can be defined by their wavelength $\lambda$, height $h$ and wave period $T$. It should be kept in mind that ocean waves are never truly harmonic. Additionally, three other parameters are often used in wave energy literature:

$$Wave\ Steepness, \quad S = h/\lambda \tag{2.1}$$

$$Wave\ Number, \quad \chi = 2\pi/\lambda \tag{2.2}$$

$$Wave\ Frequency, \quad \omega = 2\pi/T \tag{2.3}$$

Among these parameters, wave steepness is used to differentiate between linear and non-linear waves. Usually, if the wave steepness is within a value of 0.018 then the wave is considered to be linear. However, with the increase in steepness the assumption of linearity becomes less precise [14].

### 2.1.2 Regular and Irregular Waves

Airy's wave theory is the widely acceptable theory of ocean surface waves that gives sufficiently high accuracy for WEC applications [15]. Formally, with the help of this theory we can now represent wave propagation as a function of time, $t$ and position, $x$.

$$\eta\ (x,t) = \ a\sin(\omega t - x\chi) \tag{2.4}$$

where,

$\eta$ = wave free surface elevation

$a$ = wave amplitude

From equation (2.4) we can see that for a fixed position $x_0$, wave elevation is purely a function of time $t$. Assuming the origin is at the centroid of a buoy and coincides with the mean still water level. Hence, for a wave gauge located at $x_0$ distance in front of buoy, the measured wave elevation will be:

$$\eta\ (t) = \ a\sin(\omega t + x_0\chi) \tag{2.5}$$

Linear waves can also be classified into two types, regular and irregular. Harmonic regular waves are characterized by a single amplitude, frequency and wavelength.

They may also have a phase angle with respect to a chosen initial time and location. While we have represented wave elevation composed of a singule frequency, it can be a combination of multiple frequencies. These multiple frequency constituted wave are called irregular waves.

Broadly speaking, Fourier decomposition analysis allows an irregular sea wave to be represented as a sum of a large number of regular waves with different amplitudes, frequencies and directions [16]. For linear irregular waves, the response of a WEC can be easily evaluated for each individual harmonic component. These responses can be simply superimposed to get the overall response of the device. This is a very useful characteristic for WEC design and performance analysis. Brilliant investigations of water waves can be found in references [17], [18], [19], [20].

## 2.2 Wave Measurement

Ocean wave measurement is crucial to understanding the wave energy resource. Probabilistic models exist that predict sea states over a finite horizon. But, measuring the actual wave elevation is necessary where these models seem inaccurate or sufficient test data is unavailable. Moreover, it is equally important to measure wave behavior during field testing of WECs with control strategies. An important aspect of WECs is their energy generation capability that depends on how closely the WEC follows

the incoming waves. Without a suitable facility for measuring incoming wave profile, accurate estimates of energy generation capability of WECs is not possible.

### 2.2.1 Devices

Some of the typical ocean wave measuring systems are surface following buoys, resistive wave probes (commonly used in a wave tank), seabed pressure sensors, acoustic current profilers and radar (land and satellite based) [5]. The most commonly used wave measuring devices are discussed below.

#### 2.2.1.1 Surface Following Buoy

This is typically loosely moored buoy consisting of a built-in accelerometer or a Global Positioning System (GPS). The signal from the accelerometer is numerically integrated to get wave surface elevation [21]. Their inclination is also used to estimate the direction of the flow of current. However, surface following buoys do suffer several drawbacks, especially during steep and rough waves they move around unevenly and are unable to follow the waves. They are prone to damage and relatively expensive.

#### 2.2.1.2 Resistive Wave Probes

Resistive wave probes measure water level by measuring the resistance of water between a pair of parallel rods. Among resistive wave probes, two wire resistance wave probes are relatively cheap, reliable and robust. Resistive wave gauges have the following advantages [22]:

- Fast data rates
- Compatibility with large arrays
- High accuracy
- Small lead-induced errors

## 2.3 Wave Energy Subsystems

A wave energy system is a complete stand-alone system that is capable of extracting maximum energy from ocean waves. There are innumerable designs, shapes and working principles but almost all contain the same generic subsystems, essentially because of their same environment and common goal. The different subsystems and their inter-relation is presented in Figure (2.1). The main WEC subsystems are as follows.

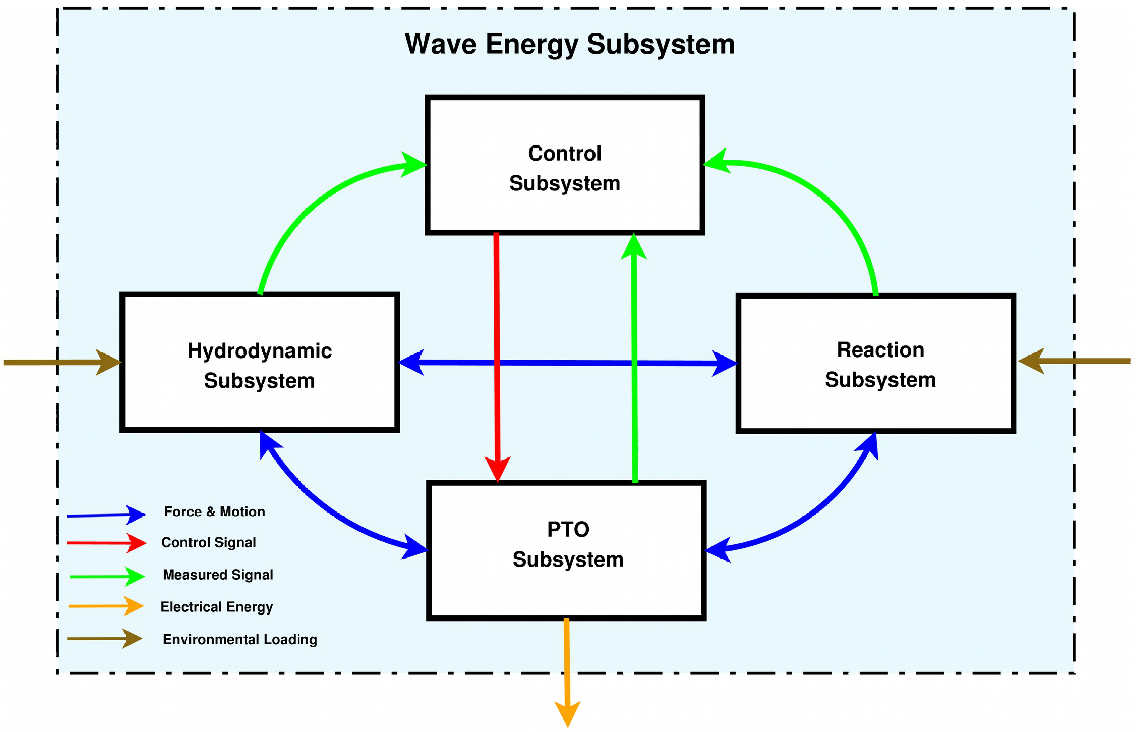


**Figure 2.1:** Wave Energy Subsystem breakdown and their correlation.

### 2.3.1 Hydrodynamic Subsystem

It is the primary wave absorption subsystem that faces the oncoming waves. It is more commonly known as a WEC. The desirable property of hydrodynamic subsystems is that it should be an effective absorber of waves. A number of methods have been proposed to classify WECs based on size (*point* absorbers and *large* absorbers), working principle and location [23]. The most widely used classification is based on the type of technology used. These include overtopping, Oscillating Water Column (OWC) and oscillating body WECs.

#### 2.3.1.1 Overtopping Converters

Overtopping converters capture the portion of waves that are at a higher elevation than its reservoir through the process of over-spilling. This stored water remains above the mean free surface level of the sea. The stored water is flown through a low-head hydraulic turbine which converts the potential energy of water to useful energy. The major drawback is that the hydrodynamics of these converters are highly nonlinear. Example of devices of this type can be found in [24].

#### 2.3.1.2 Oscillating Water Columns

Oscillating water columns, as the name suggests, are large structures of concrete or steel that are partly submerged in water. These structures are open at the bottom, trapping air above the free water surface. As the incident oscillatory waves interact with the free internal surface, it forces air through an axial flow Wells turbine. The turbine, which has an advantage of requiring no rectifying valves, drives an electric generator. These types of OWC are built and used in India [25], Portugal [26] and Norway [24]. Another type of OWC are the floating type. Their design is similar to fixed OWC except instead of being moored to the seabed, they are slack moored and can oscillate more freely. This enhances the energy extraction of this type of OWC.

#### 2.3.1.3 Oscillating Body Systems

Oscillating body systems are the most advanced form of the three types of hydrodynamic devices. They are a form of oscillating bodies either partially or fully submerged. They experience the most powerful waves when they are deployed offshore. As a result they are more complex than OWC type WECs. They are further classified as follows.

1. **Single-body Heaving Buoys**

   These are the least complex type of oscillating bouy systems. They consist of a fixed frame (sea-bottom or any other fixed structure) against which a buoy reacts in a heaving motion. Due to their small width compared to wavelength, they are also known as point absorbers.

2. **Two-body Heaving Buoys**

   One body heaving buoys may have operating difficulties due to the large distance between the sea surface and the sea-bed. This results in unnecessary forces on the mooring due to tidal oscillations. To resolve this issue, a multi-body heaving buoy can be used instead, which uses the relative motion between the upper and lower oscillating body. A detailed approach to such a system is presented in [27]. Due to the interaction between two oscillating bodies, this type of WEC possess difficult control issues as discussed in [28], [29], [30].

3. **Fully Submerged Heaving Systems**

   These devices produce energy by heave motion and are fully submerged inside the free water surface. An example of this type is the Archimedes Wave Swing (AWS) [31]. A fully submerged heaving systems consists of a fixed lower part and an oscillating upper part that moves down under a wave trough and vice versa. This oscillating motion is resisted by the interior air pressure acting as a virtual spring for a linear generator type PTO.

4. **Pitching Devices**

   Unlike the WECs previously discussed, this oscillating WEC converts wave energy into useful electrical energy through relative rotation (mostly pitch). One of the remarkable examples is the Salters duck from the University of Edinburgh [32].

5. **Bottom-hinged Systems**

   This system is a type of WEC that operates in pitch mode. It is in the form of an inverted pendulum, hinged at the bottom of the sea. An example proposed by Salter [33] is a symmetrical mace that constituted a buoyant spar capable of swinging about a universal joint. The energy extraction takes place through the rotation of a wave-activated reciprocating drum. Several cables are wound around the winch-drum in the front and back part of the WEC in the direction of wave propagation.

### 2.3.2 Power Take-Off Subsystem

PTO subsystem is responsible for applying resistance to the oscillatory motion of the hydrodynamic subsystem to convert the captured wave energy into useful electrical energy that can be supplied to the electrical grid. However, due to the variability of wave power in amplitude and time, a PTO subsystem typically requires a rectifier and a storage system. This is necessary to ensure the stringent power quality requirements at the grid are met. The oscillatory behavior of hydrodynamic subsystems results in an alternating current which is taken care of by the rectifier producing a unidirectional flow of energy. The energy storage system takes the role of decoupling random sea state and an (ideally) constant destination (grid) [34].

A maximum amount of energy is extracted by a PTO subsystem when it moves along one degree of freedom only [5]. That is why our analysis focuses on one mode i.e. heave. On the basis of this working principle, a PTO subsystem can be divided into hydraulic PTO, linear generators, air and water turbine and direct drive mechanical PTOs. The most common of these types are discussed here.

#### 2.3.2.1 Hydraulic PTO

The hydraulic PTO uses the buoy oscillatory motion to compress and decompress the fluid stored in a chamber known as an actuator [35]. These PTOs are especially suitable for slowly oscillating bodies with large wave forces and/or moments. These PTOs can accumulate energy over a couple of wave periods and thus smooth the highly variable power from the waves. A conventional electric generator is used that is driven by a fast hydraulic motor. More engineering issues and application of this PTO can be found in [36], [37]. Some configurations of PTO of this type are presented in [38], [39].

#### 2.3.2.2 Linear Generators

Unlike the hydraulic PTO, liner generators are direct driven PTOs [4]. Hence, they do not require a mechanical interface and therefore avoid associated losses in turbines and hydraulic motors. This advantage is however negated by much higher demands than high speed rotary PTOs due to higher load offering in case of direct drives [40]. The linear generator reciprocating motion has to match the buoy oscillation. The velocity in such cases is two orders of magnitude lower than the usual rotary generator velocities. This results in large forces at low speeds requiring a dimensionally large machine. An overview of direct drive PTO technologies is presented in [41], [42], [43].

### 2.3.3 Reaction Subsystem

This subsystem is used to maintain large floating WECs into position with respect to the sea bed and is deployed typically in water depths of greater than $40m$. These WECs and associated structures experience drift forces due to wind, tides and currents and hence, have to be kept in place with the help of a reaction subsystem by providing a reaction point. But unlike other structures such as oil and gas platforms, these moorings significantly modify the absorbed energy patterns by interfering with the buoy motion [44]. A detailed study comparing the type of mooring connection with WEC performance is presented in [45]. Fitzgerald et al. linearized the mooring force around the mean buoy position so that frequency domain analysis can be applied conveniently. Additionally, steps to designing mooring structures can be found in [5].

### 2.3.4 Control Subsystem

The control subsystem is the brain of the complete wave energy subsystem. It consists of the control algorithm, associated circuitry for automated and electromechanical processes, instrumentation for sensors, data acquisition, user interface, etc. The conversion of wave energy to a useful form of energy undergoes a series of energy conversion processes, each having their associated efficiency as well as some constraints.

The purpose of the control subsystem is to ensure that the hydrodynamic subsystem operates in a manner so that the wave absorber and other components meet optimal performance targets [46]. Moreover, the control subsystem should be capable of modifying control inputs in view of external disturbances on the WEC. The control input can be applied to potentially three different stages of the conversion process, either exclusively or in combination. These are hydrodynamic transmission, electric generation and power conversion [47].

# Chapter 3

# WAVE ENERGY CONVERTER CONTROL

This section provides a synopsis of the control strategies that have been used by researchers for both linear and nonlinear WEC models. In [48], a historical overview of WEC control is presented, where the authors mention the key publications that form the basis of the optimal control theory. The primary objective of any control law that focuses on maximization of power absorption in a linear system is to force the device velocity to be in phase with the excitation force [9]. Reference [49] reviewed a number of control methods applicable to heaving point absorbers. Control techniques such as linear damping, latching control, complex conjugate control (CCC), optimal velocity tracking and model-predictive control were considered. The performance

parameters for comparison were power absorption, difficulty in implementation, and maximum to average power ratio. These comparisons were made based on simulation results. The authors also commented on ways of implementing the controllers and handling buoy displacement constraints.

In order to systematically present major control strategies, the following section discusses the theory as well as some examples of implementation of different control strategies, highlighting their limitations and recent advancements.

## 3.1 Latching Control

One way to reduce the phase shift between buoy velocity and excitation force is to use discrete phase control known as latching control. It consists of a braking system that applies an ON/OFF PTO force. The braking system locks buoy displacement at one of the extreme positions (crest or trough) until a crest or trough approaches the buoy to attain maximum velocity at these extremes. The control system then re-locks the displacement for next crest or trough.

Latching control has good power absorption characteristic and a straightforward implementation in a real device because the braking force is easier to implement compared to any reactive force [13] . It also doesn't require on-board energy storage nor

involve large reactive energy exchange between the PTO and converter.

But when the incident wave is irregular, there is no well-defined phase between excitation force and velocity. The presence of more than one frequency component causes the optimal latching interval to not be unique [50]. In such cases, it was shown by [51] that for maximization of absorbed power, the optimal latching duration must synchronise the peak of excitation force with the peak of velocity. This formulation is complex due to the calculation of latching time, which requires the solving of the optimization procedure and the forecasting of incoming waves, when the latching method is used in real-time control. Moreover, there is no reactive control associated with the method of alternatively switching braking force ON/OFF. Hence, this method is generally sub-optimal as it does not lead to hydrodynamically optimum velocities [13].

Early implementation of a Kalman Filter to calculate the latching time based on estimates of incoming wave elevations was done by [52]. References [53], [54] and [55] simulated a mathematical model of a buoy with latching control. The buoy shape had a hemispherical bottom with a cylindrical top, and the experimental wave-tank results were compared with simulation results. Reference [56] also reported and compared experimental results for latching control. Latching was also experimentally tested on buoy prototypes such as SEAREV [57], [58], [59] and Buldra [60].

References [61], [62] and [63] applied several control techniques and reported the performance comparison from simulation results for an Archimedes Wave Swing. They showed that latching control and feedback linearization were able to extract maximum energy compared to reactive and phase and amplitude control. They asserted that since the two control strategies are non-causal, they require wave prediction for practical implementation, thus decreasing their effectiveness.

## 3.2 Neural Network Control

The use of Artificial Neural Network (ANN) is gaining popularity in ocean energy domain for system identification and control. Reference [64] presents the use of neural network in optimization, while [65] laid out the main steps in system identification using neural networks. Several examples of some special problems where a neural network is used in system modelling are solved in [66].

Real-time system identification of WEC dynamics was provided by [67] using ANNs. Moreover, [68] used an ANN to successfully control AWS WEC. Reference [66] used Hopfield neural network for parameter estimation and model identification. Their model had the remarkable property of estimating time varying parameters. These models can be used for WECs deployed in polychromatic waves, the parameters of

which depend on frequency of excitation. The ANN model constructs a complex relationship between input and output used to train the model. Due to the property of using only input-output observations, the ANN models are behavioral or black box models. Reference [69] solved the over-fitting problem of classical back-propagation algorithms by using a regularization procedure. Their objective function had higher identification accuracy compared to the conventional methods. To overcome the limitation posed by the black-box model characteristic of neural networks, [70] developed a *grey-box* model using ANNs. They formulated a mathematical transfer function based on an input-output of the ANN model by using network weights as coefficients of transfer function. Reference [71] developed a model-free algorithm for reactive control of a WEC. They mapped wave height, time period, PTO damping and stiffness to absorbed power and buoy displacement. This ANN was used within the cost function of a numerical optimization strategy to compute optimal damping and stiffness coefficients for maximum absorbed energy and maximum buoy displacement within prescribed limits.

One of the most pioneering work with neural networks was done by [72]. They were able to design their own specialized NN model that estimated the value of coefficients of dynamic equations. With their technique, it was possible to construct white-box models of dynamical systems. The proposed method was robust to errors in modelling or use of incomplete dynamical equations. They constructed an objective function that used the squared deviation of observation points from their simulated values

and the sum of the squared residual of dynamical equation computed at some points. Their NN weights represented actual physical quantities.

## 3.3 Model Predictive Control

Model predictive control attempts to solve a quadratic programming (QP) problem using an optimization based control strategy in a receding horizon environment [73]. MPC requires a dynamic model of the system for optimization. Theory and advancements on MPC can be found in [74]. MPC has several advantages compared to other control strategies. It is effective in performing trade-off analysis between extracted energy, energy consumed by actuator and displacement constraints. Also, the QP of its objective function can be made convex. This promotes the use of efficient optimization algorithms that are extensively developed [75]. These factors support real-time applicability of MPC while ensuring low cost of hardware. Recently, [76], [77] adopted MPC to calculate optimal latching duration for a real-time latching control. The incoming waves were forecasted using ANNs and trained by using a deep machine learning algorithm. It was shown that this combination of controller strategies increased the absorbed energy substantially. In [78] a semi-submerged sphere was considered in heave motion by the authors. They showed the effect of buoy displacement and control force constraints on extracted energy. They assumed the excitation force was known completely. Similar work was implemented by [79] on a

point absorber. The author predicted the excitation force using a Kalman filter.

## 3.4 Complex-Conjugate Control

Complex-conjugate control, also known as impedance-matching or reactive control, is a control strategy specific for maximum power absorption. It can be applied through the PTO, if the WEC is modelled as a linear system. The applied PTO force is such that the mechanical reactance of the device is cancelled by the reactance of control force. Complex-conjugate control sets a maximum bound on the amount of energy that can be absorbed by the device subject to regular waves. Hence, this strategy can be used to study the effectiveness of different modelling strategies by comparing their extracted energy.

Reference [73] compared control strategies that require current and future information of excitation force (CCC, DP, SB, MPC). For their study, they assumed that the linear hydrodynamic model is perfect and complete knowledge of the incoming wave was known for the entire simulation time. Reference [80] provides simulation and experimental results for a model of Salter duck using complex conjugate control. Reference [51] applied impedance-matching control to a sphere submerged partially in water and oscillating in heave motion only. References [81], [82] analysed complex conjugate control in presence of irregular waves.

The requirement of foreknowledge of excitation force can be obtained by a floating buoy or other measuring devices at a known distance ahead of the WEC. This technique makes it possible to apply complex conjugate control in the physical world. References [83], [84], [85], [86] laid down the requirements of accurate prediction and the negative effects of prediction errors in extracted energy. Reference [87] implemented CCC using a linear generator type PTO for polychromatic waves by tuning the PTO to match the peak frequency of the incoming wave spectrum.

## 3.5 Other Control Strategies

Reference [88] used the fuzzy logic controller for the control of WECs. Optimal PTO damping and stiffness were determined by the fuzzy logic depending upon the incoming wave profile. These optimal values were dependent on past values and adjusted in real time by measuring wave elevation. The fuzzy logic was dependent upon future incoming waves. Their work was expanded in [89] and [90] to include genetic algorithm and robust control with fuzzy logic.

Reference [91] used a time domain model for an energy maximization problem for a cylindrical buoy oscillating in heaving motion. The authors considered both regular and irregular wave spectrum. Lagrangian multipliers were used to determine the optimal force numerically. Unconstrained and constrained cases of buoy displacement

were simulated. It was found that with accurate incident wave prediction, although the total extracted energy in unconstrained case was higher, the conversion efficiency of the WEC system was better in the constrained case. Reference [35] also used Lagrangian multipliers and showed that the optimal solution converges to the CC solution with appropriate initial displacement and velocity conditions.

Reference [92] used an innovative method of reinforcement learning for the simulation and resistive control of point absorbers in regular and irregular waves. The authors used model based approach so that the algorithm was immune to modelling errors and drift in hydrodynamic parameters over time. Reference [35] used pressure distribution on WEC surface, buoy displacement and velocity to calculate the control force. This control technique was valid for linear as well as nonlinear models. They also showed that the calculation of excitation and radiation force was not required with their dynamical model approach. Reference [93] considered hydrodynamic forces and control force as system nonlinearities. Their objective was to optimize these nonlinearities by expressing them as a series function with constant coefficients. These nonlinear forces were compared with a Proportional-Derivative (PD) control. The total stiffness was considered like a proportional term and the damper was analogous to a derivative term. This approach intuitively converted a nonlinear control problem to a PD tuning problem. Hidden gene genetic algorithm was used to optimize coefficients for maximum power absorption. Reference [94] applied a control force by fitting a narrow banded function to the excitation force. They named this strategy,

simple-but-effective control. This strategy resulted in power absorption similar to MPC but was comparatively easier to implement [47].

# Chapter 4

# DYNAMIC MODELLING

The basic principles governing motion of buoys in water are derived from the theory of marine hydrodynamics. These governing equations first developed in the 1950s for the purpose of predicting the behavior of vessels and boats when placed in ocean waves. Detailed and exhaustive description of theory developed in the field of hydrodynamics in this period is mentioned in [95].

A body close to the surface of fluid and capable of absorbing the incident waves also has the ability to affect the oncoming wave field. As the body oscillates in water, it generates its own waves and these waves along with incident waves apply a net force on the body [13]. These forces acting on a body immersed in a fluid depend on the properties of fluid, which are defined by its pressure and flow velocity. Standard

fluid dynamic equations apply and are used for development of necessary governing equations. The fluid is assumed to be incompressible to express mass conservation in the form of a continuity equation. Secondly, to solve Navier-Stokes equation, the incident flow is taken as inviscid and irrotational. Finally, surface tension at the interface is assumed negligible [96]. The inertial frame is assumed to be fixed at stationary water level (SWL) and origin at the centroid of body which coincides with the gravitational center. A SDOF floating buoy for wave energy conversion in heave motion is shown in figure (4.1). The lower side of the buoy is connected to a linear generator type PTO which is then anchored to the sea bed. Waves propagate in the x-direction and follow a sinusoidal profile. Different modes identified based on this coordinate system are presented in Table 4.1.

**Table 4.1**
Different modes of motion identified with respect to the coordinate system located at the centroid of buoy with $x$ in the direction of wave propagation and $z$ is the vertical motion.

| **Mode** | **Translation** | **Rotation** |
|---|---|---|
| Surge | X | - |
| Sway | Y | - |
| Heave | Z | - |
| Roll | - | X |
| Pitch | - | Y |
| Yaw | - | Z |

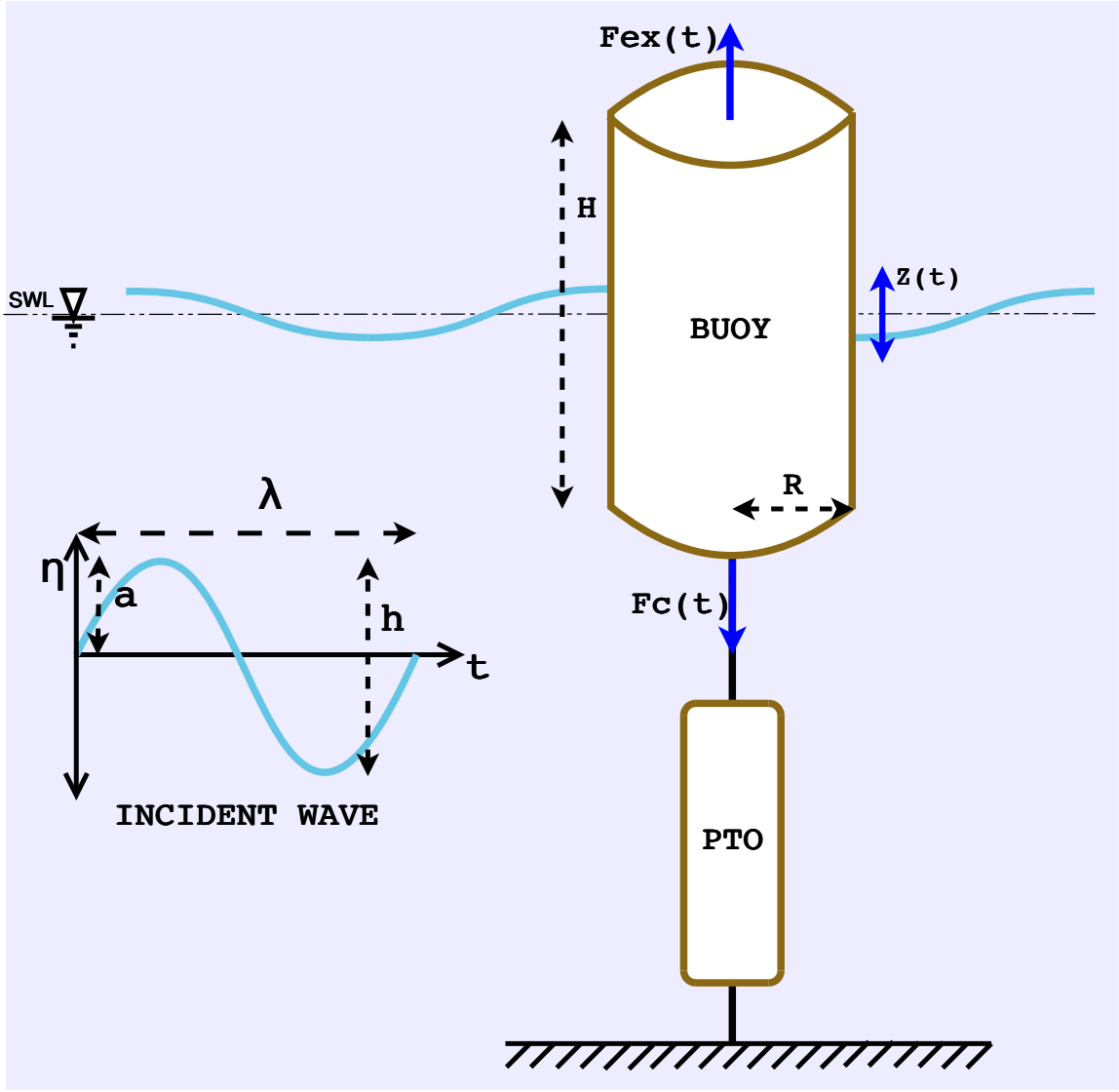


**Figure 4.1:** Heaving buoy with power take-off unit moored to the sea floor. Incident waves are along $x$ - axis with $\lambda$ wavelength and $a$ elevation.

A general and simplified description of how the WEC hydrodynamic model is developed for heave motion is presented along with necessary assumptions that establish its validity. A complete description of derivation for a multi degree of freedom WEC can be found in books of marine hydrodynamics and/or wave energy conversion [97],

[98].

## 4.1 Types of Forces

For a single body oscillating in a fluid in heave motion, the governing equation is:

$$m\ddot{z} = F_d + F_r + F_{FK} - F_c \tag{4.1}$$

Where $m$ is the mass of the buoy in air, $z$ is the vertical displacement of the body from the mean position ($z = 0$) and positive upwards, $F_d$ is the diffraction force, $F_r$ is radiation force, $F_{FK}$ is the total Froude-Krylov force and $F_c$ is applied PTO (external control) force. The direction of control force is taken opposite to diffraction force arbitrarily. These forces are discussed below:

### 4.1.1 Diffraction Force

It is the force that the approaching wave field applies on the buoy, assuming the buoy is not oscillating (i.e. held stationary) in water. In some literature, diffraction force is frequently called scattering force. It is calculated by integrating the diffraction

pressure, $P_d$ over the submerged area of the body.

$$F_d = \int \int_S P_d \, \mathbf{n} \, dS \tag{4.2}$$

Where,

$P_d = \rho \, \dfrac{\partial \phi_d}{\partial t} + \rho \, \dfrac{|\nabla \phi_d|^2}{2}$

$\phi_d$ = Diffraction potential

$S$ = Submerged buoy area

$n$ = Unit vector normal to surface area

Another way of representing the diffraction force is by convolving the product of the free surface elevation and the diffraction impulse response function (IRF).

$$F_d \, (t) = \int_{-\infty}^{+\infty} K_{d_{irf}}(t - \tau) \, \eta(t) \, d\tau \tag{4.3}$$

Where,

$K_{d_{irf}}$ = Diffraction IRF

### 4.1.2 Radiation Force

It is the force that acts on the body when it oscillates in calm water. It is the sum of added mass effect and the convolution between the product of WEC velocity and the radiation IRF [7]. It can be represented as:

$$F_r\ (t) = \ -\int_{-\infty}^{+\infty} K_{irf}(t-\tau)\ \dot{z}(t)\, d\tau - m_a\, \ddot{z} \tag{4.4}$$

Where,

$K_{irf}$ = Radiation IRF

$m_a$ = Added mass (including frequency-independent component)

During implementation, it is very expensive to evaluate this convolution integral at each time step. Moreover, it is not feasible in real time control. Hence, [99], [100] presented a method to approximate the convolution integral using a state space realization.

$$\dot{\vec{x}}_r = \mathbf{A}_r \vec{x}_r + \mathbf{B}_r v \tag{4.5}$$

$$\vec{F}_r = \mathbf{C}_r \vec{x}_r \tag{4.6}$$

Where,

$$\mathbf{A}_r = \begin{bmatrix} 0 & 0 & 0 & \dots & 0 & -a_1 \\ 1 & 0 & 0 & \dots & 0 & -a_2 \\ 0 & 1 & 0 & \dots & 0 & -a_3 \\ \vdots & \vdots & \vdots & \ddots & \vdots & \vdots \\ 0 & 0 & 0 & \dots & 0 & -a_{n-1} \\ 0 & 0 & 0 & \dots & 1 & -a_n \end{bmatrix}$$

$$\mathbf{B}_r = \begin{bmatrix} p_1 & p_2 & p_3 & \dots & p_{n-1} & -p_n \end{bmatrix}^T$$

$$\mathbf{C}_r = \begin{bmatrix} 0 & 0 & 0 & \dots & 0 & 1 \end{bmatrix}$$

$\vec{x}_r$ = Radiation state vector

$v$ = Input heaving velocity of buoy

This state space has a companion form realization with $2n$ unknown parameters. Such state space representation has an impulse response function [101] of the form given by :

$$g_r(t) = \mathbf{C}_r \, e^{\mathbf{A}_r t} \, \mathbf{B}_r \tag{4.7}$$

For the given state space to represent the convolution integral of equation (4.4), it is necessary and sufficient that $K_{irf}(\mathrm{t}) = g_r(\mathrm{t})$. The equality holds for an infinite order state space, but a sufficiently higher order can be made to approximate the

convolution integral closely. This state space can be converted to a radiation damping transfer function $G_r$(s) that can be represented as:

$$G_r(s) = \frac{p_{n-1}\, s^{n-1} \ + \cdots \ + p_1\, s}{s^n \ + a_{n-1}\, s^{n-1} \ + \cdots \ + a_1\, s \ + a_0} \tag{4.8}$$

Reference [102] discusses state space estimation of the convolution term in detail for a raft-type WEC.

### 4.1.3 Froude-Krylov Force

Froude-Krylov force is the net hydrodynamic force acting on the body due to unsteady pressure fields. It consists of two parts, hydrostatic force $F_{FK_{st}}$ and hydrodynamic force $F_{FK_{dy}}$. The $F_{FK_{st}}$ is the difference between gravity and buoyant force, whereas $F_{FK_{dy}}$ is the surface integral of dynamic pressure over instantaneous wetted area. Mathematically,

$$F_{FK_{st}}\,(t) = F_g \ - \int\int_S P_{st}\,(t)\ \mathbf{n}\, dS \tag{4.9}$$

$$F_{FK_{dy}}\,(t) = \ - \int\int_S P_{dy}\,(t)\ \mathbf{n}\, dS \tag{4.10}$$

where the Hydrodynamic pressure is, $P_{dy} = \rho\, \dfrac{\partial \phi_i}{\partial t} \ + \rho\ \dfrac{|\nabla \phi_i|^2}{2}$

Hydrostatic pressure, $P_{st} = \ -\rho\, g\, z$

$\phi_i$ = Incident flow potential

$g$ = Acceleration due to gravity

## 4.2 Linear Model

The general model presented in the previous section has three main sources of nonlinearities. First, the quadratic terms in pressure from the Bernoulli's equation, second, the incident waves can be nonlinear and third, the instantaneous wetted area of the WEC is time-varying. Falnes [98] showed that the quadratic terms in pressure are negligible compared to the linear terms and hence, can be dropped. The second nonlinearity can be neglected if the analysis only considers linear waves, as they constitute the majority of waves in the region of power production. Lastly, a mean value of wetted surface can be calculated for a specific geometry and taken as a constant in the analysis. With these assumptions, equation (4.1) can be written for a linear model as:

$$m\ddot{z} = \int_{-\infty}^{+\infty} K_{d_{irf}}(t-\tau)\ \eta(t)\,d\tau\ - \int_{-\infty}^{+\infty} K_{irf}(t-\tau)\ \dot{z}(t)\,d\tau\ - m_a\,\ddot{z} + F_g\ - \int\int_S P_{st}\,(t)\ \mathbf{n}\,dS\ - \int\int_S P_{dy}\,(t)\ \mathbf{n}\,dS\ - F_c \quad (4.11)$$

Which can be written in the form given by Cummins,

$$(m + m_a)\,\ddot{z} = \int_{-\infty}^{+\infty} K_{e_{irf}}(t-\tau)\;\eta(t)\,d\tau \;- \int_{-\infty}^{+\infty} K_{irf}(t-\tau)\;\dot{z}(t)\,d\tau \quad - K_h\,z \;- F_c \tag{4.12}$$

or

$$(m + m_a)\,\ddot{z} = F_{ex} \;- \int_{-\infty}^{+\infty} K_{irf}(t-\tau)\;\dot{z}(t)\,d\tau \quad - K_h\,z \;- F_c \tag{4.13}$$

where,

$F_{ex} = \int_{-\infty}^{+\infty} K_{e_{irf}}(t-\tau)\;\eta(t)\,d\tau = \int_{-\infty}^{+\infty} K_{d_{irf}}(t-\tau)\;\eta(t)\,d\tau \;+ F_{FK_{dy}}$

$F_{FK_{dy}} = -K_h\,z$

$K_h$ = Hydrostatic stiffness

$K_{e_{irf}}$ = Excitation IRF

The convolution of the product of the excitation IRF and the free surface elevation is called the excitation force, $F_{ex}$. It is the combination of the diffraction force and the dynamic Froude-Krylov force. For low frequencies, the diffraction force is small compared to the dynamic Froude-Krylov force [98].

## 4.3 Non-Linear Model

As already stated in the development of the linear model, the wetted area of the buoy varies with time. Calculation of the dynamic Froude-Krylov force is based on this instantaneous wetted area and usually requires discretization of the buoy's surface geometry into a fine mesh. The force on each elemental area is found by summing the pressure force. As the body moves in the next time step, the wetted area changes and the re-meshing and force calculation procedure has to be repeated. It is possible to write a re-meshing routine that does this job automatically at each time step, but the process will be highly computationally expensive. However, Giorgi et al. presented a method to calculate dynamic Froude-Krylov force based on instantaneous wetted area for common buoy geometries for heave motion [9]. The proposed algebraic solution had 2% error compared to re-meshing routine approach. The reason for deviation was due to non-ideal discretized geometry in the re-meshing case. It was also found that no algebraic solution exists for motion with a combination of heave and pitch.

Meriguad et al. [103] found that the most prominent of the nonlinearities affecting the response of the buoy with a non-uniform cross sectional area is the nonlinear Froude-Krylov force. The device dynamics has negligible effect due to nonlinear radiation and diffraction forces. To corroborate their results, Guerinel et al performed real wave tank experiments and compared them with results from the nonlinear model

[104]. Their nonlinear model used linear diffraction and radiation forces and nonlinear Froude-Krylov forces. The results agreed with experimental values.

Another nonlinear factor that Giorgi and Ringwood [105] considered in their model was nonlinear viscous damping, which they compared with a fully nonlinear CFD model. The nonlinear viscous damping term was modelled by using Morrison's equation [106]:

$$F_{vis} = \frac{1}{2}\,\rho\, C_d\, A_d\ \mid \dot{z}\ -\dot{\eta}\mid\ (\dot{z}\ -\dot{\eta}) \tag{4.14}$$

Where,

$F_{vis}$ = Viscous force

$C_d$ = Drag coefficient

$A_d$ = Characteristic surface area

The magnitude of drag coefficient determines the intensity of the viscous damping, which requires computational fluid dynamics (CFD) simulations or experimental wave tank testing. Using $F_{FK_{nonlin}}$ for total nonlinear Froude-Krylov force, the complete nonlinear model can be described by the equation below:

$$(m+m_a)\,\ddot{z} = F_d\ + F_{FK_{nonlin}}\ - \int_{-\infty}^{+\infty} K_{irf}(t-\tau)\ \dot{z}(t)\,d\tau\ \ - K_h\,z\ - F_c\ - F_{vis} \tag{4.15}$$

## 4.4 Wave Energy

Just like energy calculation for wind turbines, the control strategies associated with WECs focus on maximizing a function of the form:

$$E = \int_{t_0}^{t} F_c \, \dot{z} \, dt \tag{4.16}$$

Where,

$E$ = Useful energy converted/absorbed by the PTO.

This absorbed energy can be expressed in the form of instantaneous power ($P$) as $P = dE/dt$. The period of useful ocean waves varies between 3-9 seconds [107]. As a result, the input power from a PTO also varies continuously. If no power smoothning device is used, the output power supplied to the grid will also show the same fluctuations. Hence, there exists a need to balance instantaneous power flow from the WEC generators. Reference [108] integrated battery energy storage (BES) with a WEC to smooth out the output power. To improve the power quality of WEC farms, design and use of back-to-back converters was suggested. Additional converter schemes are given in [109], [110], [111]. Use of auxiliary electrical stages ensures that the frequency of the generator is decoupled from the fixed voltage and frequency of the grid. Hence, the WEC generator can operate at variable speeds.

# Chapter 5

# DESIGN and METHODOLOGY

This chapter discusses individual hydrodynamic effects along with their mathematical models. These effects are eventually combined to form a governing equation used for creating the energy optimal solution. Assumptions are provided that distinguish the linear and nonlinear models. Finally, performance criteria to evaluate success of proposed model with design of cases for hypothesis testing is presented.

## 5.1 Statement of Hypothesis and its Selection

It has been firmly established that for WECs to be successful on a large scale, energy flow from PTOs to the grid needs to be maximized. Moreover, it is understood that

nonlinear models are better at predicting buoy dynamics compared to the linear models especially when buoy motion is large or buoy cross sectional area is not constant [104]. There is a need for linear modelling method that is as accurate as a nonlinear model, so that well-documented real-time optimal control strategies can be applied to this proposed model for accurate extracted energy estimations. It is hypothesized that the optimal force from the proposed model would result in more extracted energy compared to optimal force from the Cummins' model. A Cummins' model is used for comparison because of its accuracy, extensive results in the literature [112], [113] and ease of calculation using WAMIT [114]. It should also be noted that from now onwards, the proposed model is called the linear estimated model.

## 5.2 Complete Model Description with Assumptions

In this section, a complete description of Cummins' and nonlinear hydrodynamic model is presented.The buoy is modelled as a vertical cylinder with radius, $R = 1m$, draft, $h_d = 2m$ and height, $H = 4m$. Incident linear monochromatic waves are assumed that induce buoy oscillation in only heave mode. A linear generator directly coupled with the buoy applies a reaction force depending on the direction of current in its coils. Boundary Element Method (BEM) [114] is used to calculate

hydrodynamic loads in the frequency domain by solving the flow problem around the geometry. Suitable selection of options for the input Force Control (FRC) files output added mass, damping coefficient, diffraction and Froude-Krylov forces. Similar to the approach of [112], the excitation force for the Cummins' model is taken as the sum of the diffraction and Froude-Krylov forces. For the nonlinear model, the Froude-Krylov force is calculated algebraically using formulations given in [9]. No nonlinear viscous force is considered in this study because Merigaud et al. [103] found that the most prominent nonlinearity affecting the buoy heave response is the nonlinear Froude-Krylov force. As previously stated, the device dynamics have a negligible effect due to nonlinear radiation and diffraction forces, hence these two forces are kept the same for the Cummins' and nonlinear model. Buoy size and meshing used in WAMIT are shown in figure (5.1). In this study, for faster computation, a transfer function was used to approximate the convolution integral of Equations (4.13), (4.15) similar to [99]. Finally, the Cummins' (5.1) and nonlinear (5.2) model take the form:

$$(m + m_a(\omega))\,\ddot{z} = F_{ex} \; - K_h\, z \; - c\dot{z} \; - F_c \tag{5.1}$$

$$(m + m_a(\omega))\,\ddot{z} = F_d \; + \pi R^2 \rho\, g\, (a \sin(\omega t)\, e^{\chi\,(z\; - h_d)} \; - z) \; - c\dot{z} \; - F_c \tag{5.2}$$

where,

$\pi R^2 \rho\, g\, (a \sin(\omega t)\, e^{\chi\,(z\; - h_d)} \; - z)$ = Nonlinear algebraic Froude-Krylov force

$c$ = Radiation damping coefficient

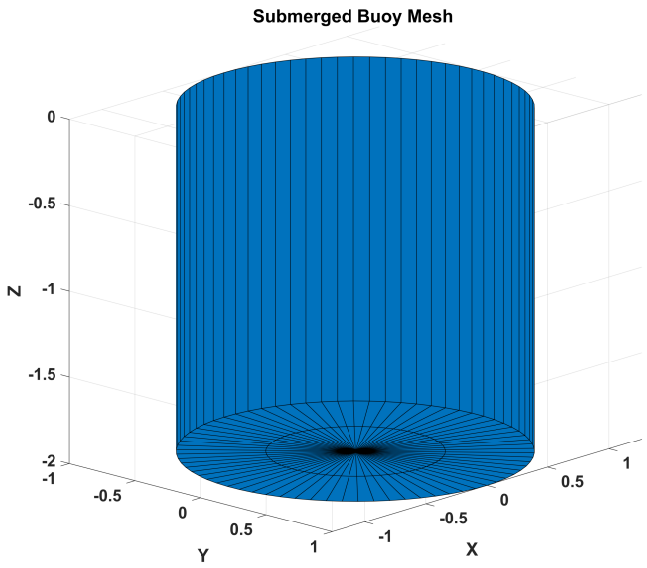


**Figure 5.1:** Submerged buoy dimension and meshing used in WAMIT.

## 5.3 Nonlinear Optimal Control Force Calculation and its Limitation

The hydrodynamic model considering nonlinear Froude-Krylov force is accurate at estimating buoy motions for regular and irregular shapes. Formulation of the general optimal force for this nonlinear model is logically the first step to calculate the theoretically possible maximum extracted energy. Due to the assumptions made in the Cummins' model, there is a difference between nonlinear and linear model based maximum energy. There is scope of capturing this energy difference if an optimal force is applied to the nonlinear model. The following derivation presents the general form of nonlinear optimal solution and necessary conditions to ensure optimality.

Nonlinear model:

$$(m + m_a(\omega))\,\ddot{z} = F_d \; + \pi R^2 \rho\, g\, (a \sin(\omega t)\, e^{\chi\,(z\; - h_d)} \; - z) \; - c\dot{z} \; - F_c \tag{5.3.1}$$

Assuming:

$m + m_a = M$

$\pi R^2 \rho\, g = Q$

If we define,

$z_1 = z,\; z_2 = \dot{z} = \dot{z_1},\; z_3 = t,\; \dot{z_3} = 1$

the equation (5.3.1) becomes

$$\dot{z_1} = z_2 \tag{5.3.2}$$

$$\dot{z_2} = \frac{1}{M}\left[F_d \; - Q\,\left(z_1 \; - a \sin(\omega z_3)\, e^{\chi\,(z_1\; - h_d)}\right) \; - c z_2 \; - F_c\right] \tag{5.3.3}$$

$$\dot{z_3} = 1 \tag{5.3.4}$$

The optimal control problem for regular waves is defined as:

Find $F_c^*$ that minimizes

$$E\,(z\,(t), F_c\,(t)) = -\int_0^{t_f} F_c\; z_2\,(t)\; dt \qquad \text{subject to (5.3.3).}$$

The Hamiltonian, $\mathcal{H}$ is defined as:

$\mathcal{H}(z_1,\; z_2,\; z_3,\; \lambda_1,\; \lambda_2,\; \lambda_3,\; F_c) = -F_c\, z_2 \; + \lambda_1\, \dot{z}_1 \; + \lambda_2\, \dot{z}_2 \; + \lambda_3\, \dot{z}_3$

$$\mathcal{H} = -F_c\, z_2 \; + \lambda_1\, z_2 \; + \frac{\lambda_2}{M}\left[F_d \; - Q\,\left(z_1 \; - a\sin(\omega z_3)\; e^{\chi\,(z_1\; - h_d)}\right) \; - cz_2 \; - F_c\right] \; + \lambda_3$$

where, $\vec{\lambda} = \begin{bmatrix}\lambda_1 & \lambda_2 & \lambda_3\end{bmatrix}^T$ are Lagrange multipliers.

The optimal control, $F_c^*$, must satisfy the necessary conditions

$$\dot{z}_i = \frac{\partial \mathcal{H}}{\partial \lambda_i}$$

$$\dot{\lambda}_i = -\frac{\partial \mathcal{H}}{\partial z_i} \qquad \lambda(t_f) = 0$$

$$\frac{\partial \mathcal{H}}{\partial F_c} = 0$$

Evaluating these conditions, we find that the optimal solution must satisfy equation (5.3.3) in addition to:

$$\dot{\lambda}_1 = \frac{\lambda_2}{M}\, Q\,\left(1 \; - a\,\chi\,\sin(\omega z_3)\; e^{\chi\,(z_1\; - h_d)}\right) \tag{5.3.5}$$

$$\dot{\lambda}_2 = F_c \; - \lambda_1 \; + \frac{\lambda_2}{M}\, c \tag{5.3.6}$$

$$\dot{\lambda}_3 = \frac{\lambda_2}{M}\, Q\,\left(-\, a\,\omega\,\cos(\omega z_3)\; e^{\chi\,(z_1\; - h_d)}\right) \tag{5.3.7}$$

$$z_2 \; + \frac{\lambda_2}{M} = 0 \tag{5.3.8}$$

As we observe from the equations above, $\mathcal{H}$ is linear in $F_c$ and the matrix $\mathcal{H}_{F_cF_c}$ is singular. Therefore the control force $F_c$ cannot be determined from $\mathcal{H}_{F_c} = 0$.

Reference [115] derived most general form of the generalized Legendre-Clebsch condition (5.3.9). It can be used to check if $F_c^*$ that maximizes $\mathcal{H}$ is an optimal solution.

$$(-1)^k \frac{\partial}{\partial F_c} \left[ \left( \frac{\partial}{\partial t} \right)^{2k} \mathcal{H}_{F_c} \right] \geq 0 \tag{5.3.9}$$

$k \in 0, 1, 2, \ldots, n$

Equation (5.3.9) is always satisfied as long as equality in equation (5.3.8) is maintained. This poses a strict requirement on the initial condition for displacement and velocity. If those initial conditions are violated, the solution is not optimal.

Differentiating equation (5.3.8) we can write,

$$\dot{z}_2 + \frac{\dot{\lambda}_2}{M} = 0$$

Using equation (5.3.8) in (5.3.5)

$$\dot{\lambda}_1 = -z_2 \, Q \left( 1 - a \, \chi \, \sin(\omega z_3) \, e^{\chi \, (z_1 \, - h_d)} \right) \tag{5.3.10}$$

Integrating equation (5.3.10)

$$\lambda_1 = -Q \left( z_1 - a \, \chi \int z_2 \, \sin(\omega z_3) \, e^{\chi \, (z_1 \, - h_d)} \, dz_3 \right) - \psi$$

where, $\psi$ is a constant of integration.

Assuming, $I = \int z_2 \ \sin(\omega z_3) \ e^{\chi \ (z_1 \ - h_d)} \ dz_3$ we get,

$$\lambda_1 = -Q \ (z_1 \ - a \, \chi I) \ - \psi \tag{5.3.11}$$

Using equation (5.3.8) and (5.3.11) in (5.3.6)

$$\dot{\lambda}_2 = F_c \ + Q \ (z_1 \ - a \, \chi I) \ + \psi \ - c z_2 \tag{5.3.12}$$

Using equation (5.3.3) in (5.3.12)

$$\dot{\lambda}_2 = F_d \ - Q \left( z_1 \ - a \sin(\omega z_3) \ e^{\chi \ (z_1 \ - h_d)} \right) \ - c z_2 \ - M \dot{z}_2 \ + Q \ (z_1 \ - a \, \chi I) \ + \psi \ - c z_2$$

Simplifying yields,

$$- \psi = F_d \ - Q a \left( \chi I \ - \sin(\omega z_3) \ e^{\chi \ (z_1 \ - h_d)} \right) \ - 2 c z_2 \tag{5.3.13}$$

Differentiating and rearranging equation (5.3.13) gives,

$$2 c \dot{z}_2 = \frac{\partial F_d}{\partial z_3} \ + Q a \omega \cos(\omega z_3) \ e^{\chi \ (z_1 \ - h_d)} \tag{5.3.14}$$

Using equation (5.3.3) in (5.3.14)

$$F_c{}^* = F_d - Q\left(z_1 - a\sin(\omega z_3)\ e^{\chi\,(z_1\ -h_d)}\right) - cz_2 - \frac{M}{2c}\ \frac{\partial}{\partial z_3}\left[F_d + Qa\sin(\omega z_3)\ e^{\chi\,(z_1\ -h_d)}\right] \tag{5.3.15}$$

Equation (5.3.15) gives the optimal control force for a cylindrical buoy when the algebraic form of nonlinear Froude-Krylov force is considered. Equation (5.3.15) can be generalized for any buoy shape to calculate the closed form of optimal control force.

For a general non-linear governing equation of the form

$$(m + m_a)\ddot{z} = \ F_d + F_{FK_{dy}} + F_{FK_{st}} - c\dot{z} - F_c$$

Optimal control force will be

$$F_c{}^* = \ F_d + F_{FK_{dy}} + F_{FK_{st}} - c\dot{z} - \frac{m + m_a}{2c}\ \frac{\partial}{\partial t}\left[F_d\ + F_{FK_{dy}}\right] \tag{5.3.16}$$

On reducing the generalized optimal force in equation (5.3.16) for the linear Cummins' equation, it matches exactly with results in [34].

To derive the required initial condition, use equation (5.3.15) in (5.3.3)

$$\ddot{z} = \frac{1}{2c}\left[\frac{\partial F_d}{\partial t}\ + Qaw\cos(\omega t)\ e^{\chi\,(z\ -h_d)}\right]$$

On integrating, we get

$$\dot{z} \ - \dot{z}_0 = \frac{1}{2c} \left[ F_d(t) \ - F_d(0) \ + Qaw \ \int_{t_0}^{t} \cos(\omega t) \ e^{\chi \ (z \ - h_d)} \ dt \right]$$

The above equation is implicit in displacement and velocity and no closed form solution was found. Numerical optimization was used to find the initial conditions for maximum energy extraction, but the results required buoy initial displacement and velocity values that were very large and physically unrealizable and hence, discarded. No solution existed within physical bounds.

This limitation of the implicit relation in displacement and velocity is overcome by replacing the nonlinear model with a linear estimate and then using the well-documented closed form optimal solution.

## 5.4 Proposed Estimated Model

It is found that application of nonlinear optimal force requires evaluation and satisfaction of implicit initial conditions for maximum energy absorption. In case they are not satisfied, it renders the use of closed form of optimal force. To overcome this drawback, the nonlinear model is estimated with a linear model such that the calculation of optimal force and initial conditions does not require solution of implicit relations. It is possible to use optimization algorithms such as Genetic algorithm for determining constrained optimal force, but it is computationally very expensive and

hence, unsuitable for real-time implementation. To qualify as a potential candidate for modelling WEC dynamics, the estimated linear model has to satisfy the following stringent requirements.

1. The estimated linear model has to be accurate compared to the Cummins' model in predicting WEC motion (displacement and velocity).

2. The implementation of estimated model should be physically realizable without high computational cost.

3. The estimated model must be capable of capturing extra energy resulting from the difference between linear and nonlinear buoy motion.

In real-world application, following steps need to be followed for the development of the estimated model.

1. Gather data for buoy motion (displacement and velocity) for a frequency band of incoming waves. This step should be repeated for a number of estimation frequency bands. Hence, the expected wave frequency region can be divided into a discrete finite number of frequency bands.

2. Fit a linear model to determine the unique set of mass, damping and stiffness for each frequency band using multiple data sets for better approximation.

3. Generate a mass, damping and stiffness matrix corresponding to incoming wave frequency similar to frequency dependent added mass and radiation damping generated by WAMIT.

## 5.5 Time Domain Model and Control Application

To test the hypothesis, same control strategy is applied to the Cummins' and the linear estimated model. The control force from both these models are used in the nonlinear model describing the actual WEC dynamics. The extracted energy from both control force cases is compared for a number of scenarios to evaluate the effectiveness of the proposed technique. This method of applying control force from two different models is used because in real-world application, the actual WEC dynamics are independent of the model used. Only the calculation of control force is affected by the choice of model used to estimate WEC displacement and velocity. Hence, comparison of extracted energy by application of different control force is indicative of which model results in larger power flow from waves to the grid.

Simulink model used to generate displacement and velocity data for parameter estimation is shown in Figure (5.2). In this case, no control force is assumed on the nonlinear model. The estimated mass, stiffness and damping are denoted by $m_{est}$, $k_{est}$ and $c_{est}$ respectively. For the same diffraction force ($F_d$), the nonlinear (5.5.1)

and estimated model (5.5.2) responses are approximately equal.

$$F_d = M\ddot{z} \ + c\dot{z} \ - Q\ (\eta\ e^{\chi\ (z\ -h_d)} \ - z) \tag{5.5.1}$$

$$F_d = m_{est}\ddot{z} \ + c_{est}\dot{z} \ + k_{est}z \tag{5.5.2}$$

Defining,

$$F_{FK_{est}} = (M \ - m_{est})\ddot{z} \ + (c \ - c_{est})\dot{z} \ + (Q \ - k_{est})z \tag{5.5.3}$$

Using $F_{FK_{est}}$ from Equation (5.5.3), the linear estimated model (5.5.2) can be represented in the form shown in Equation (5.5.4) which is an estimated linear model of Equation (5.5.1).

$$M\ddot{z} = F_d \ + F_{FK_{est}} \ - c\dot{z} \ - Qz \tag{5.5.4}$$

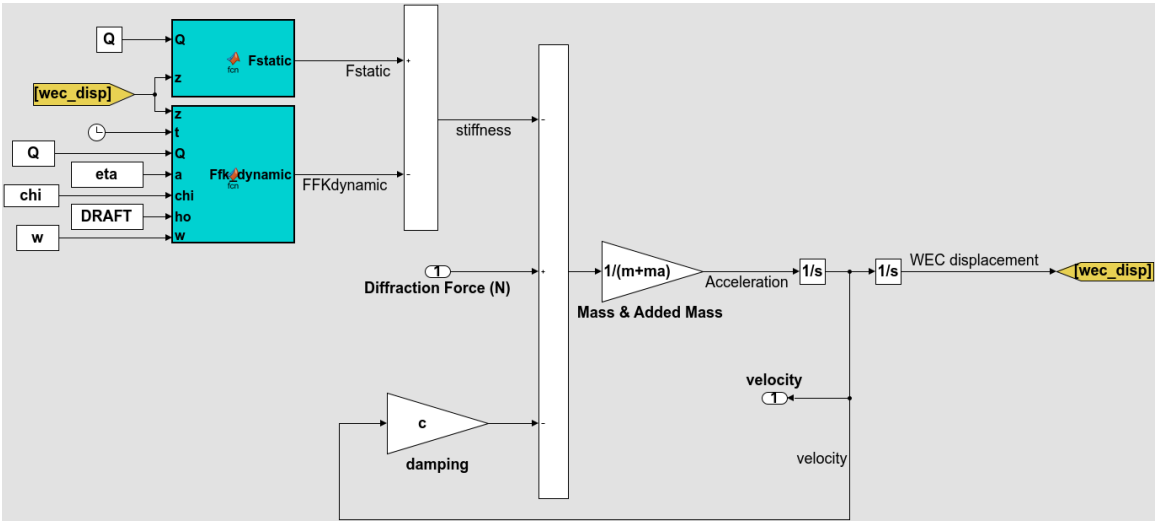


**Figure 5.2:** Nonlinear model used to generate displacement and velocity data for parameter estimation.

Time domain model used for control law application is shown in Figure (5.3). Diffraction ($F_d$) and excitation forces ($F_{ex}$) are shown as an output of a sinusoidal block, calculated as described in Sections 4.1.1 and 4.2 respectively. Governing equations and control law for each block is stated below:

**Nonlinear model**: From Equation (5.3.3) we have,

$$M\ddot{z} = F_d \ + Q\ (\eta\ e^{\chi\ (z\ -h_d)}\ - z)\ - c\dot{z}\ - F_c \tag{5.5.5}$$

**Cummins' model**: Equations (5.1) and (5.3.16) are used to represent the governing equation (5.5.6) and control law (5.5.7) respectively as shown below:

$$M\ddot{z} = F_{ex}\ - K_h\, z\ - c\dot{z}\ - F_{c_{cummins}} \tag{5.5.6}$$

$$F^*_{c_{cummins}} = F_{ex}\ - K_h\, z\ - c\dot{z}\ - \frac{M}{2c}\ \frac{dF_{ex}}{dt} \tag{5.5.7}$$

**Linear estimated model**: Equations (5.5.4) and (5.3.16) are used to represent the governing equation (5.5.8) and control law (5.5.9) respectively as shown below:

$$M\ddot{z} = F_d \ + F_{FK_{est}}\ - c\dot{z}\ - Qz\ - F_{c_{linear}} \tag{5.5.8}$$

$$F^*_{c_{linear}} = F_d \ + F_{FK_{est}}\ - c\dot{z}\ - Qz\ - \frac{M}{2c}\ \frac{d(F_d + F_{FK_{est}})}{dt} \tag{5.5.9}$$

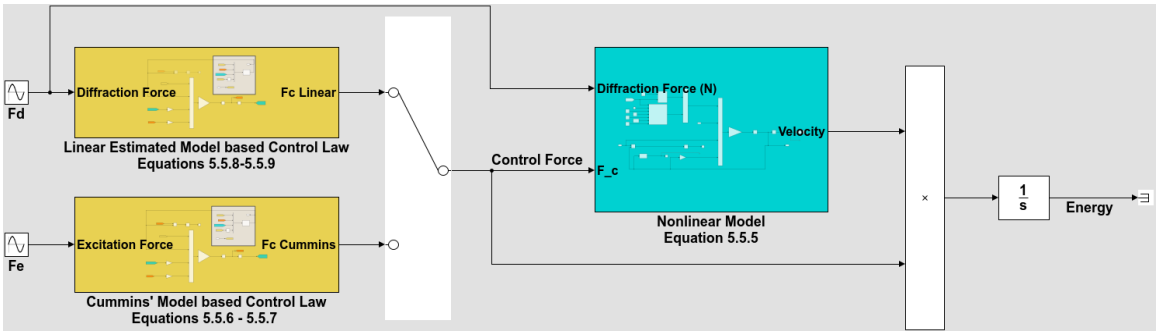


**Figure 5.3:** Time domain model showing application of optimal control force based on either Cummin's model or Linear estimated model.

Based on which model to use for energy extraction, control force can be switched from the Cummins' model to the linear estimated model.

## 5.6 Design of Experiment/Test Cases

In order to encompass maximum sea states, an approach close to [9] is followed. Two wave steepness indices (0.018 & 0.012) are considered where the higher steepness corresponds to the limiting value allowed in the linear wave regime. For each steepness, two target wave periods are selected for parameter estimation. These two periods lie at the opposite ends of a range of time periods commonly experienced by a point absorber in deep water conditions [116]. The selected wave periods are 4 and 8 seconds. Moreover, to ensure physical realization of the proposed technique, each set of parameters is estimated for a band of frequencies lying in the vicinity of the targeted time

period. Two such bands are studied, $-/+0.5$ and 0.1 seconds and three frequencies are selected from each band for estimating one set of parameters. The choice of the time period band was made keeping in mind two factors. A 0.5 second band ensures a limited number of tests to cover the whole expected wave frequency domain, while a 0.1 second band helps to analyze the benefits of accurate parameter estimation. Finally, for each case, two kinds of incident waves are tested. The period of the first wave lies within the band for which parameters were estimated and the period of the other wave is far off. A layout of these different test cases is also presented in figure (5.4).

## 5.7 Hypothesis Testing

It is important to carefully design methodology for testing the hypothesis such that an unbiased assessment of the estimated model in terms of the aforementioned requirements can be performed. Four different types of evaluation criteria have been used to test the estimated model against Cummins' model in terms of accuracy, extracted energy and robustness. These criteria are explained in detail below:

1. Responses of the estimated and Cummins' model were compared with the non-linear model for several incident wave frequencies when no control force was applied. This ensured the estimated model was accurate at frequencies other

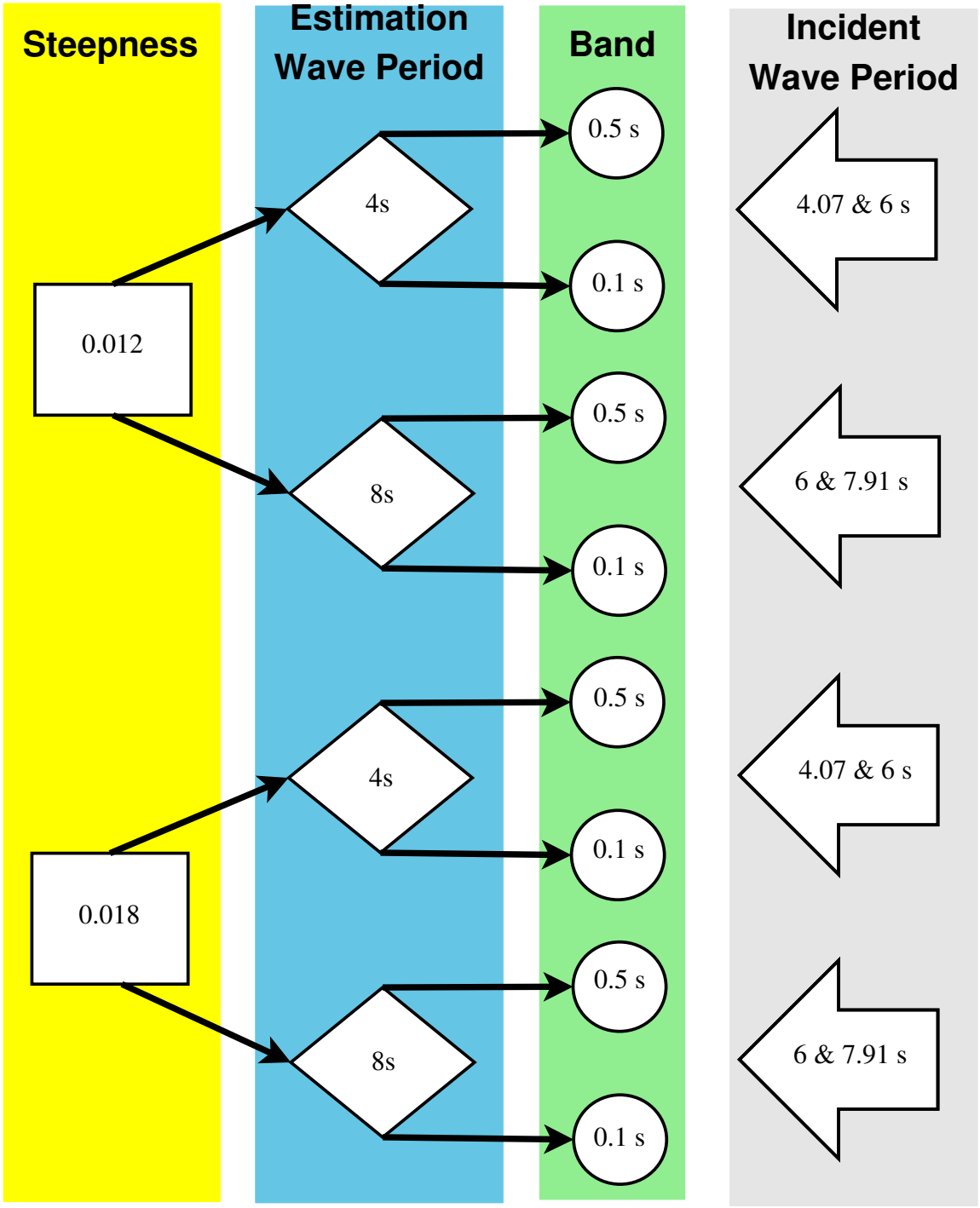


**Figure 5.4:** Layout showing combination of steepness, estimation wave period and incident wave period used to generate different test cases.

than those used for estimation.

2. Extracted energy was compared when the control force was given by the Cummins' and the estimated model. This showed there was an optimal force other than calculated from Cummins' model which results in higher energy extraction from the nonlinear model.

3. The effect of bandwidth of frequencies used to estimate one set of parameters was compared against extracted energy. This gave an indication of appropriate size of frequency band used for estimation.

4. The extracted energy was compared in cases where the incoming wave frequency was outside the band used for parameter estimation. This illustrated robustness of the estimation model to extreme waves or in cases where insufficient data collection resulted in incomplete modelling for the whole frequency domain.

## 5.8 Explanation of Technique/ Data Collection

This section explains the procedure for setting up simulation, data collection, estimation and calculation of extracted energy for each test case.

1. Simulation Setup

   (a) Select geometry of prototype buoy and obtain its mesh from NEMOH.

(b) Convert NEMOH mesh file to geometry file for use in WAMIT.

(c) Run WAMIT to obtain added mass, radiation coefficients, FRC file, hydrostatic stiffness, etc. in the frequency domain.

(d) Compute radiation convolution in time domain and approximate with a state space/transfer function.

(e) Compute IRF for excitation force from FRC file.

2. Data Collection

(a) Selection of wave frequency and steepness for estimation.

(b) Choose a frequency band and select three frequencies within the band.

(c) Determine diffraction force for each of the three frequencies by convoluting diffraction IRF and wave elevation.

(d) Use nonlinear model governed by equation (5.2) for generating buoy motion data (displacement and velocity).

3. Parameter estimation

(a) A linear model was used to satisfy three sets of input output relation using interior point optimization method (fmincon). It was found that fmincon performed better in reducing error than parameter estimation toolbox in Simulink.

4. Energy calculation

(a) Choose an arbitrary incident wave frequency and one of the two steepness.

(b) Determine wave elevation and compute excitation and diffraction forces from convolution.

(c) Use excitation force in Cummins' model and diffraction force in the estimated model and calculate the optimal force.

(d) Apply optimal force from both models into nonlinear model to compare energy extracted.

# Chapter 6

# RESULTS and CONCLUSIONS

This chapter is divided into six sections. The first four sections present the results to evaluate the efficacy of the estimated model against the Cummins' model on four criteria. Sections 5 and 6 present conclusion and future work respectively.

## 6.1 WEC Motion with no Control Force

Figures (6.1), (6.2), (6.3), (6.4), (6.5), (6.6), (6.7) and (6.8) show the steady state displacement and velocities of the WEC using three different models. In all graphs, the dashed black line shows the nonlinear motion. Green marker and solid blue lines are used to show model responses for the $-/+0.1s$ and $-/+0.5s$ time period

bandwidth estimated models. The solid red lines show results obtained from the Cummins' model when no control force is applied. The incident wave frequencies used for testing the no-control force behavior were chosen arbitrarily to cover the entire expected frequency span and were different from those used to estimate the linear model parameters. Four cases were considered, as described in Table (6.1). Cases - 1 and 2 consider incident wave with frequencies within the region used for parameter estimation while Cases - 3 and 4 consider wave frequencies outside the estimated region. Incident waves in Cases - 2 and 4 have lower steepness compared to Cases - 1 and 3. For each case, comparison of both displacement and velocity is presented. This is important because the model should predict accurate displacement and velocity. This ensures it can accurately estimate energy extraction. Also, for each case, small amount of distortion in the sinusoidal velocity response is observed for the nonlinear model response. This causes higher percentage amplitude difference (PAD) in velocity compared to displacement.

**Table 6.1**
Wave Steepness and Time period corresponding to each Case.

| **Case** | **Excitation force** | | **Average Time Period used for estimating Linear model** |
|---|---|---|---|
| | **Steepness** | **Time period (s)** | |
| 1 | 0.018 | 4.07 | 4 |
| 2 | 0.012 | 7.91 | 8 |
| 3 | 0.018 | 6 | 8 |
| 4 | 0.012 | 6 | 4 |

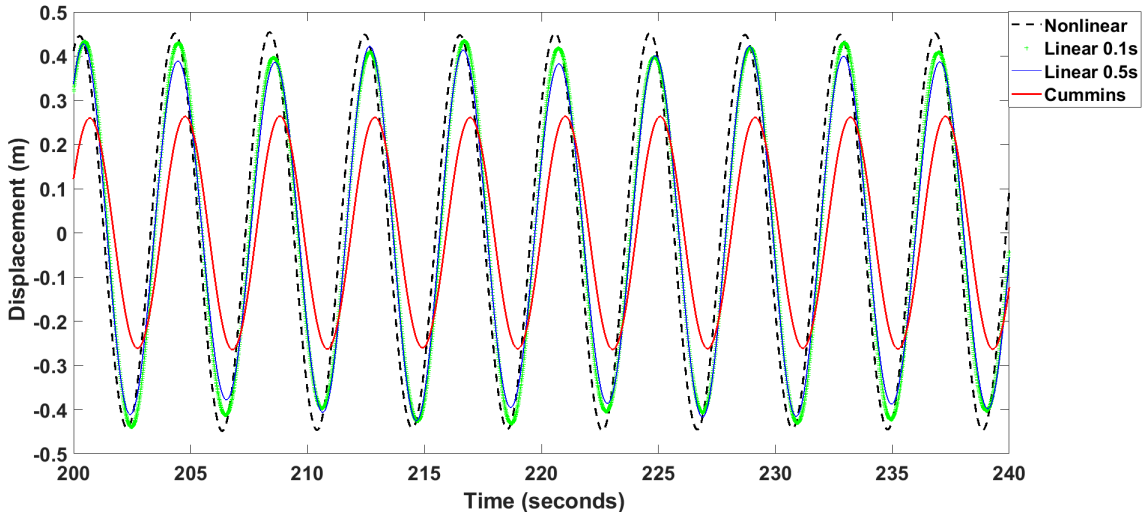


**Figure 6.1:** Case - 1a. Comparison of the nonlinear, linear estimated and Cummins' model displacement without control force. The incident wave has high steepness (0.018). Time period ($4.07s$) lies inside the parameter estimation bandwidth.

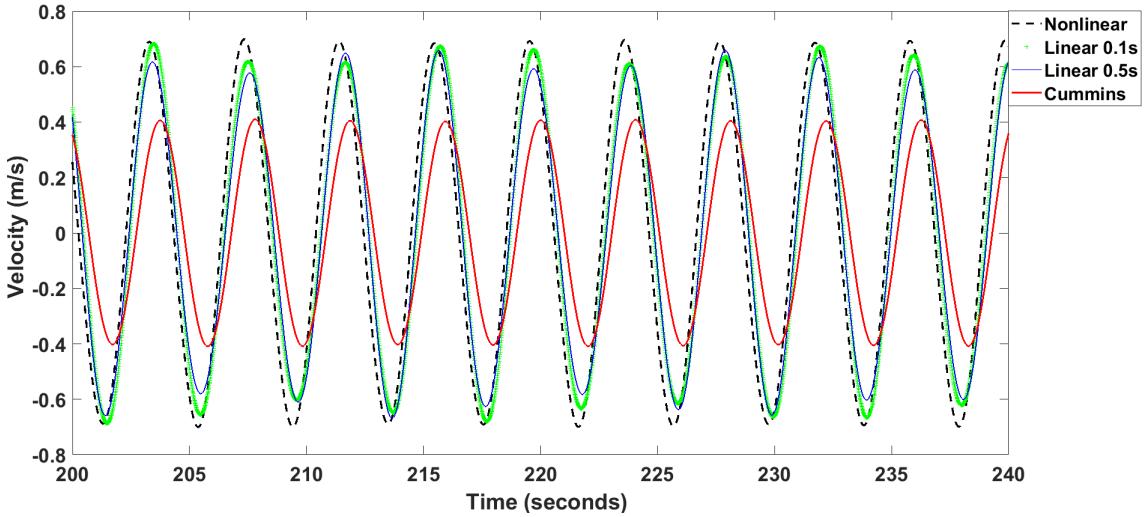


**Figure 6.2:** Case - 1b. Comparison of the nonlinear, linear estimated and Cummins' model velocity without control force. The incident wave has high steepness (0.018). Time period ($4.07s$) lies inside the parameter estimation bandwidth.

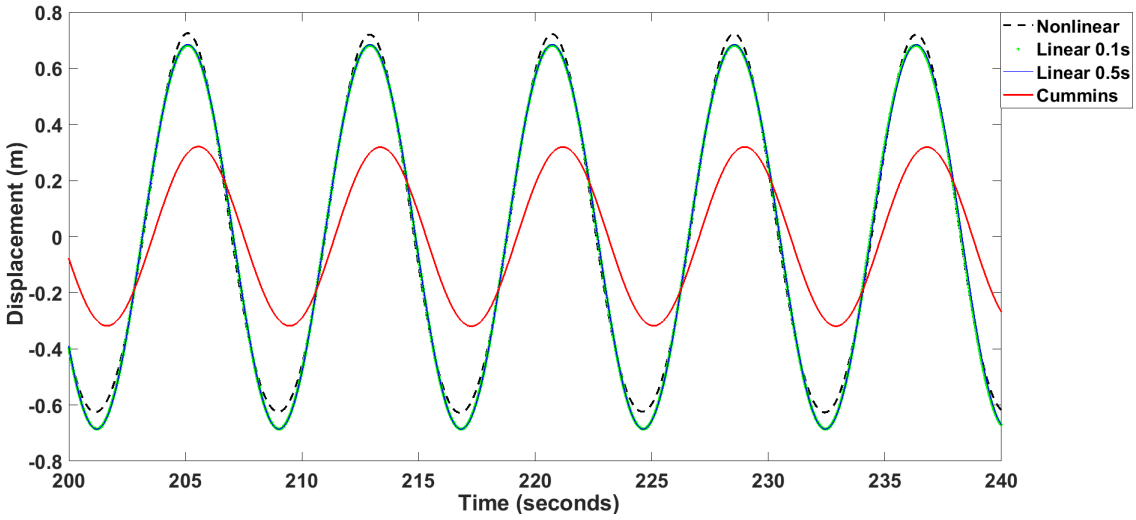


**Figure 6.3:** Case - 2a. Comparison of the nonlinear, linear estimated and Cummins' model displacement without control force. The incident wave has low steepness (0.012). Time period (7.91$s$) lies inside the parameter estimation bandwidth.

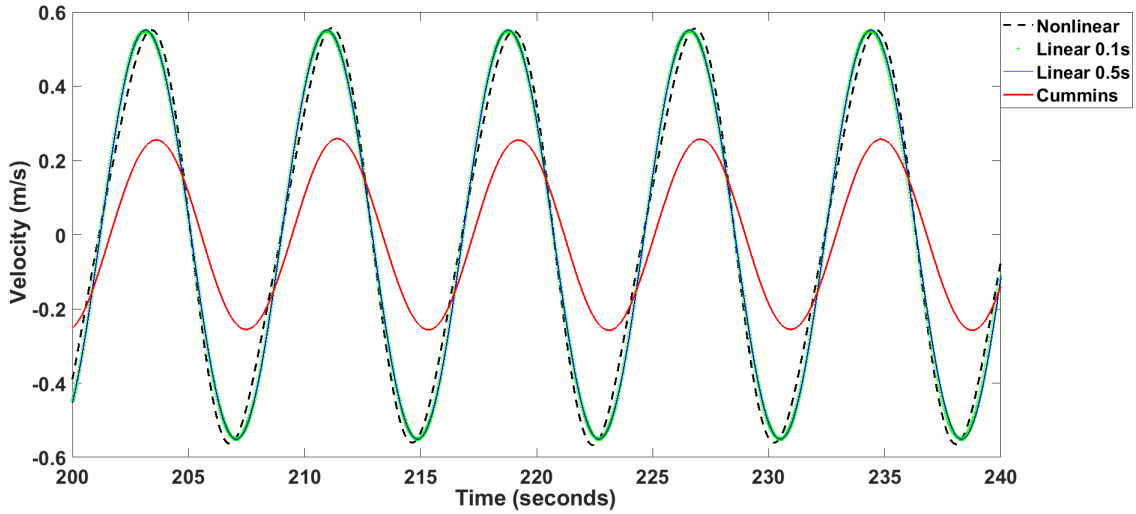


**Figure 6.4:** Case - 2b. Comparison of the nonlinear, linear estimated and Cummins' model velocity without control force. The incident wave has low steepness (0.012). Time period (7.91$s$) lies inside the parameter estimation bandwidth.

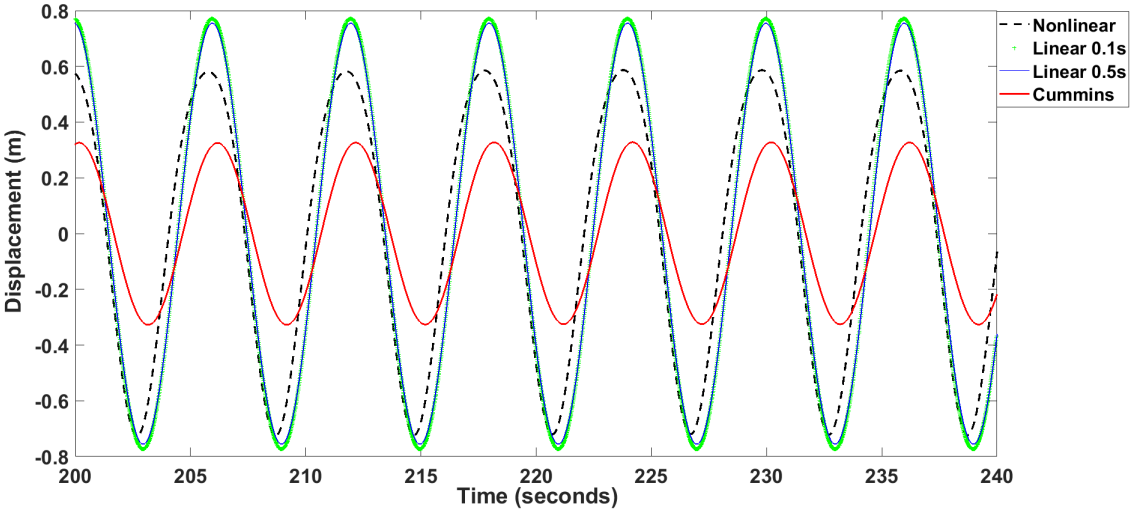


**Figure 6.5:** Case - 3a. Comparison of the nonlinear, linear estimated and Cummins' model displacement without control force. The incident wave has high steepness (0.018). Time period ($6s$) lies outside the parameter estimation bandwidth.

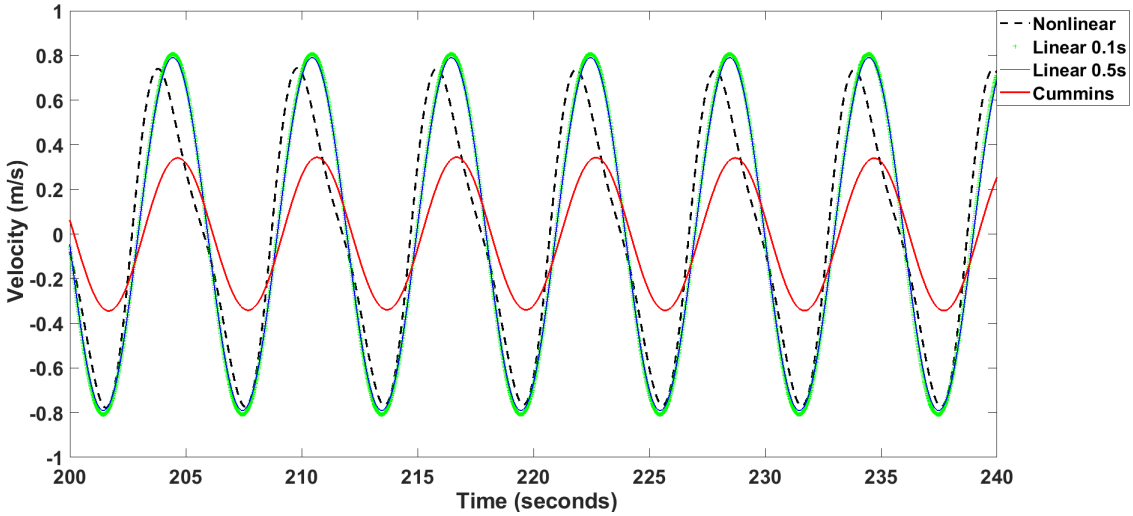


**Figure 6.6:** Case - 3b. Comparison of the nonlinear, linear estimated and Cummins' model velocity without control force. The incident wave has high steepness (0.018). Time period ($6s$) lies outside the parameter estimation bandwidth.

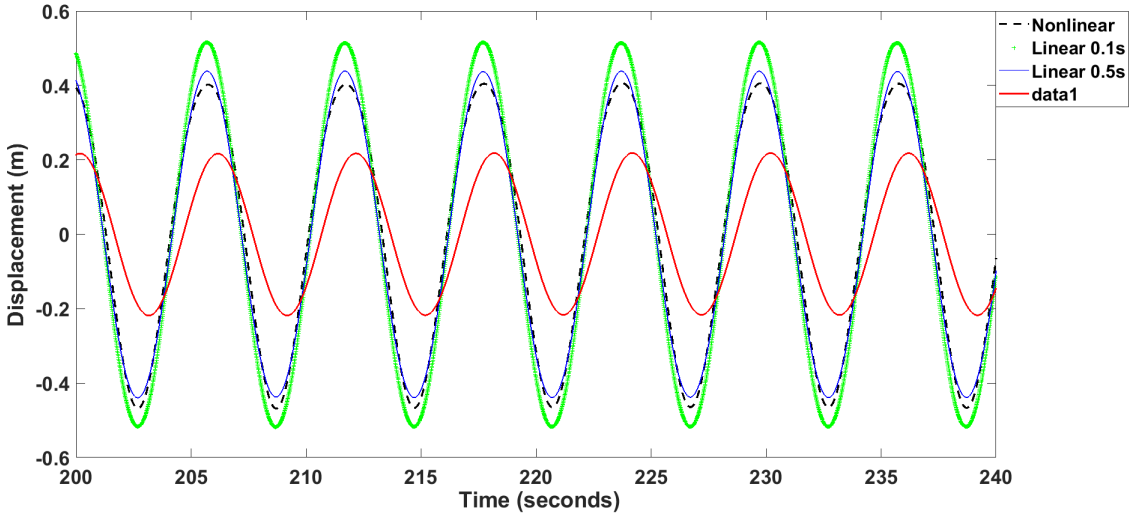


**Figure 6.7:** Case - 4a. Comparison of the nonlinear, linear estimated and Cummins' model displacement without control force. The incident wave has low steepness (0.012). Time period ($6s$) lies outside the parameter estimation bandwidth.

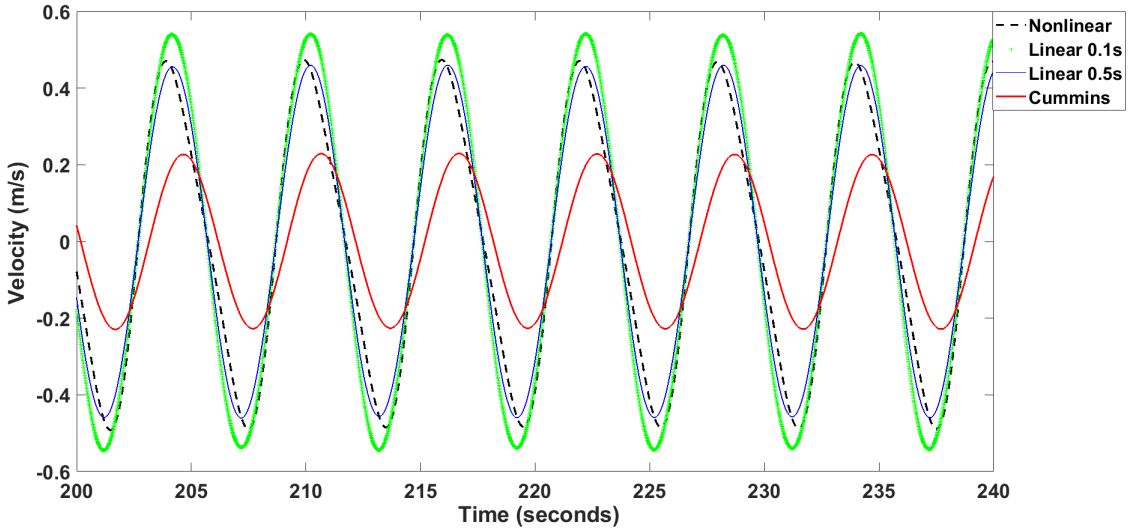


**Figure 6.8:** Case - 4b. Comparison of the nonlinear, linear estimated and Cummins' model velocity without control force. The incident wave has low steepness (0.012). Time period ($6s$) lies outside the parameter estimation bandwidth.

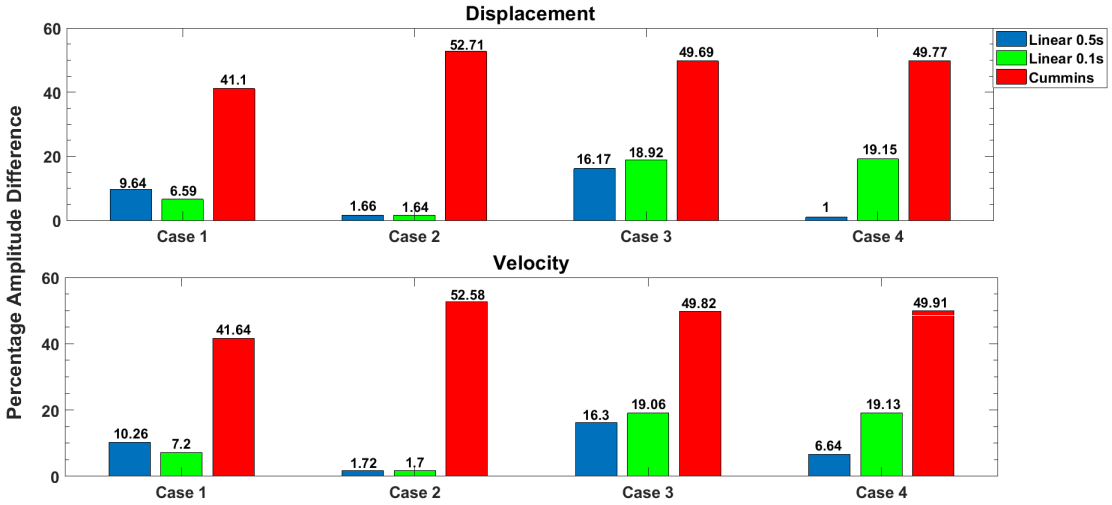


**Figure 6.9:** Comparison of Percentage Amplitude Difference of the Linear versus Cummins' model with respect to the Non-Linear model.

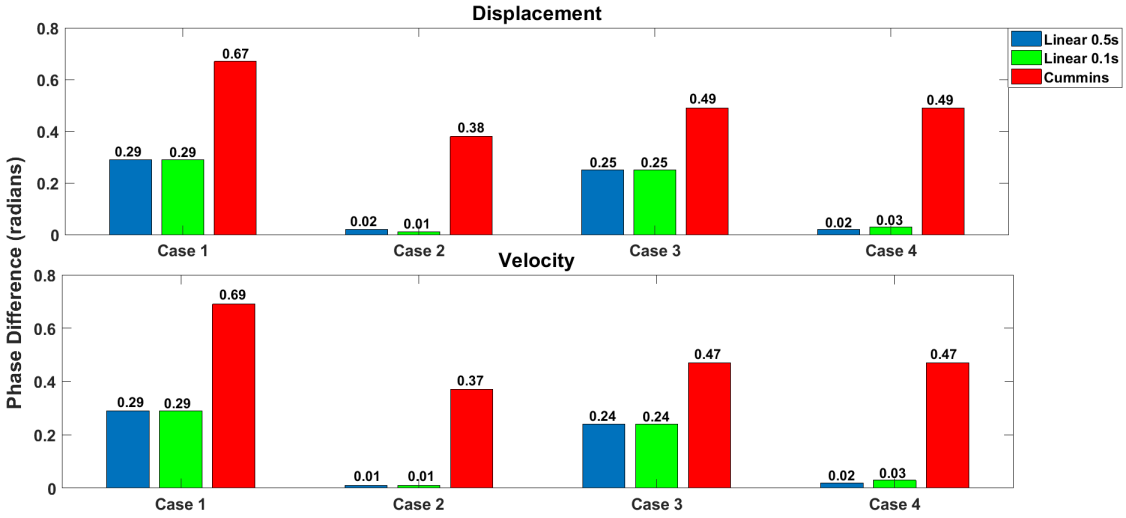


**Figure 6.10:** Comparison of phase difference (radian) of the Linear versus Cummins' model with respect to the Non-Linear model.

It can be seen graphically that the estimated model outperforms the Cummins' model in predicting WEC motion. Numerical comparison of phase and amplitude difference for each case is presented in Figures (6.9) and (6.10) respectively. For each case,

the Cummins' model has higher amplitude and phase difference compared to the linear model. It is also observed that when the incident wave is within the prediction region (Cases 1 and 2), the narrower $(+/-0.1s)$ bandwidth model has lower PAD compared to the wider $(+/-0.5s)$ bandwidth model. The reason lies in the estimation process. As three sets were used to estimate the model parameters for each bandwidth, narrower bandwidth resulted in precise estimation for that region. Hence, when the excitation frequency lies in that region, the narrower bandwidth model shows better correlation with the nonlinear model. Opposite behavior is observed when excitation frequency lies outside of the two $(+/-0.5s$ and $+/-0.1s)$ estimation bandwidth regions (Cases 3 and 4). This is because, initially the model was estimated for a wider range of frequencies. As a result, its parameters were more accurate at extraneous incident frequencies. However, from Figure (6.10) we observe that phase difference remains constant when two models with different estimation frequency bandwidths (Linear 0.1s and Linear 0.5s) were compared with the nonlinear model (ex. Case 1).

## 6.2 Extracted Energy Comparison

Figures (6.11), (6.12), (6.13), (6.14), (6.15), (6.16), (6.17) and (6.18) show the extracted energy comparison between control laws based on the estimated versus the Cummins' model. Here, solid blue and red lines show the extracted energy by application of control force from the linear estimated model with -/+ 0.5 and

0.1 second bandwidth respectively.The energy extracted by applying control force from the Cummins' model is shown by solid yellow color lines. In this section, the linear and Cummins' model are used to calculate the control force by using Equations (5.5.6 - 5.5.9). The response in Section 6.1 is completely different from cases presented here as no control law was used in Section 6.1. Eight cases are shown. Cases 5, 6, 7 and 8 consider high steepness (0.018) waves, whereas Cases 9, 10, 11 and 12 face low steepness (0.012) incident waves. For Cases 5,8,9 and 12, the incident wave frequency is inside the parameter estimation bandwidth and for the rest of the Cases, it lies outside. Table 6.2 shows energy extracted (in megajoule) at the end of a 200 second time span for each of the test Cases.

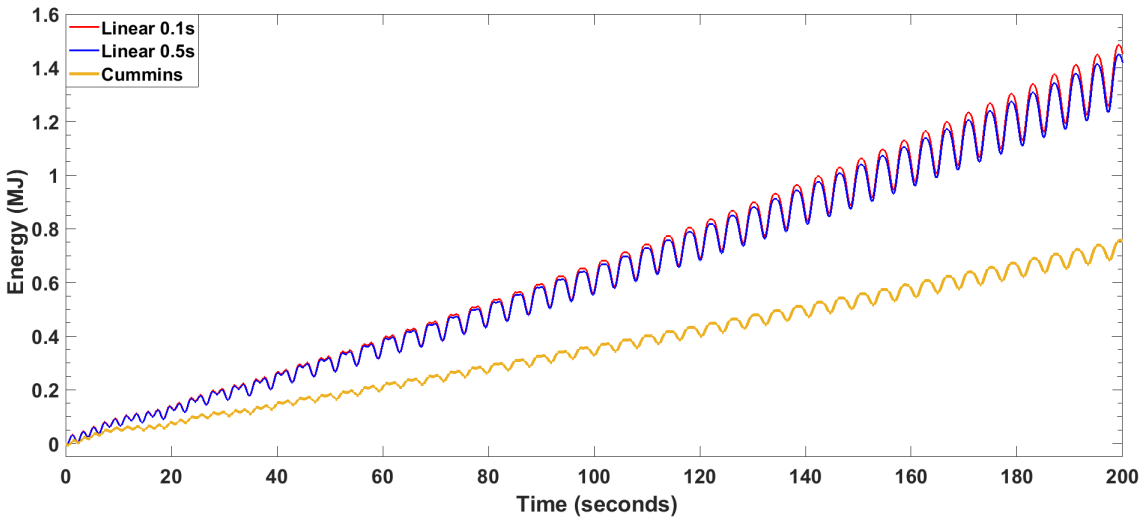


**Figure 6.11:** Case - 5. Comparison of extracted energy between the Linear estimated and Cummins' model. Incident wave with high steepness (0.018). Time period ($4.07s$) lies inside the parameter estimation bandwidth (3.9s - 4.1s).

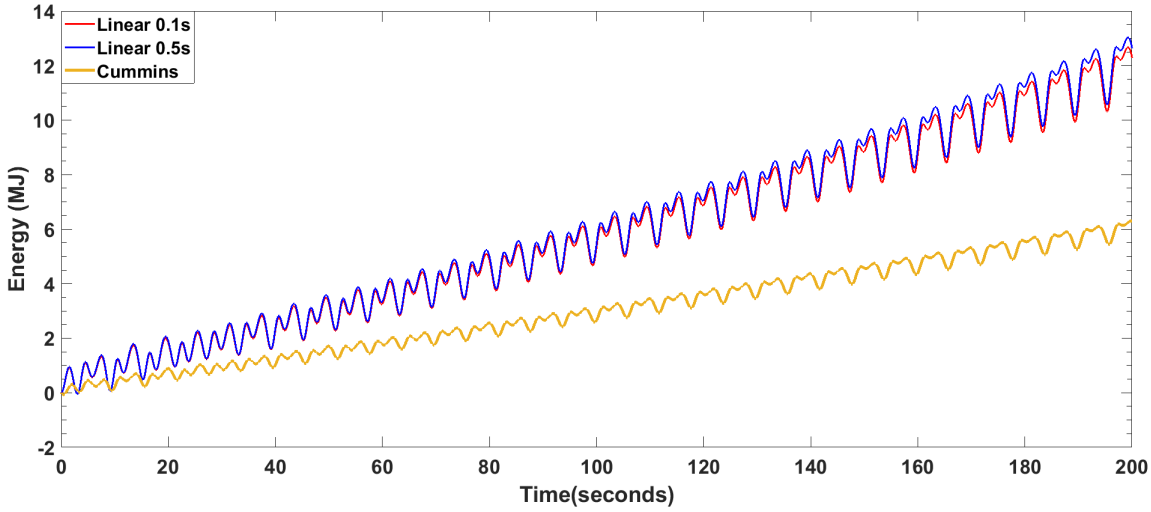


**Figure 6.12:** Case - 6. Comparison of extracted energy between the Linear estimated and Cummins' model. Incident wave with high steepness (0.018). Time period ($6s$) lies outside the parameter estimation bandwidth (3.9s - 4.1s).

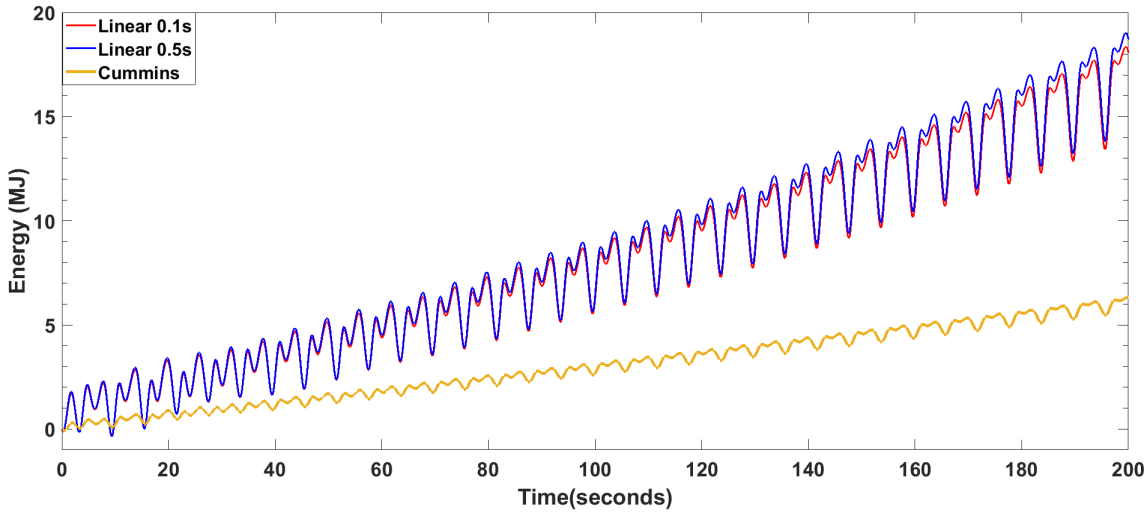


**Figure 6.13:** Case - 7. Comparison of extracted energy between the Linear estimated and Cummins' model. Incident wave with high steepness (0.018). Time period ($6s$) lies outside the parameter estimation bandwidth (7.9s - 8.1s).

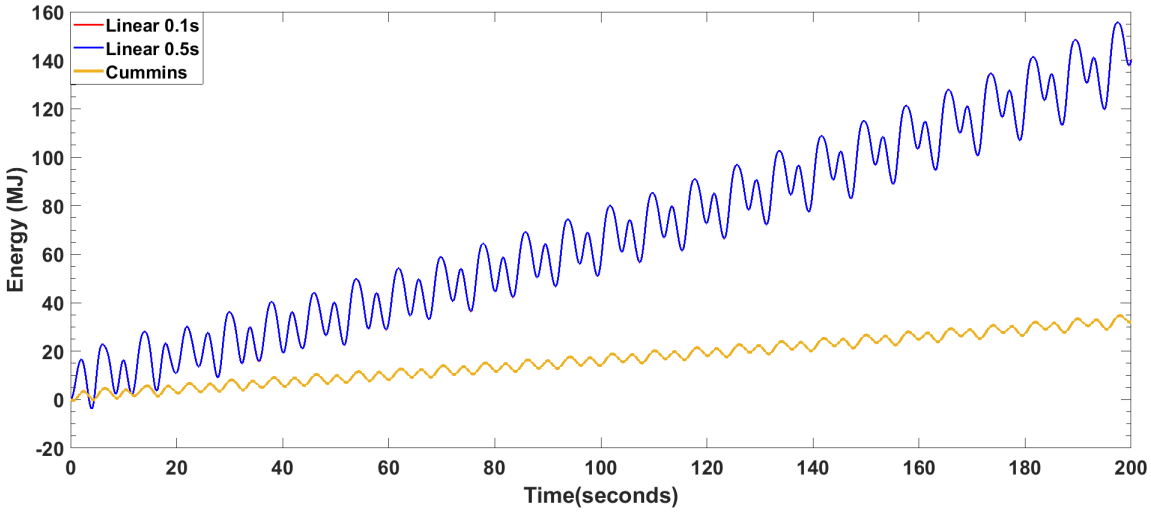


**Figure 6.14:** Case - 8. Comparison of extracted energy between the Linear estimated and Cummins' model. Incident wave with high steepness (0.018). Time period (7.91$s$) lies inside the parameter estimation bandwidth (7.9s - 8.1s).

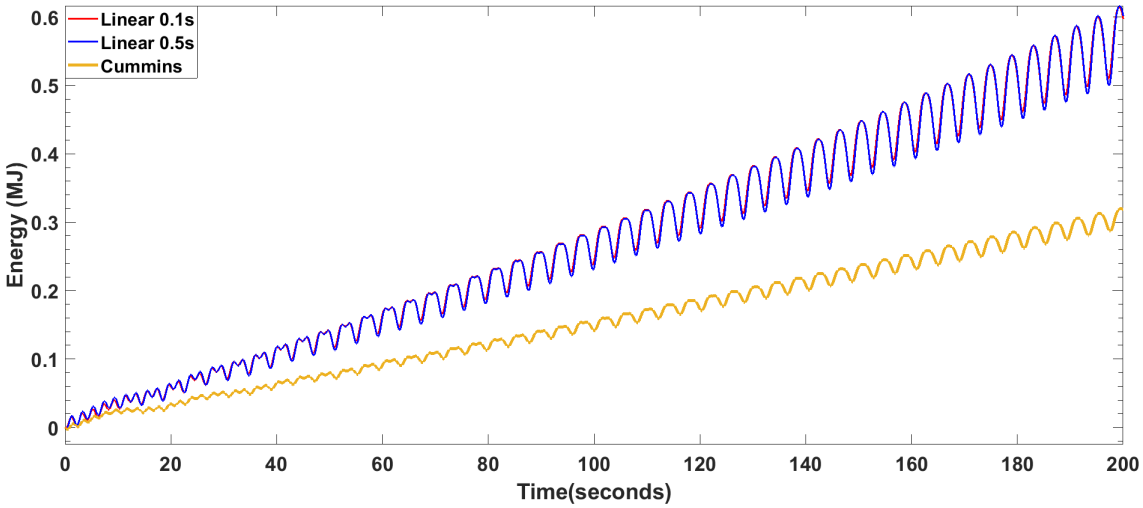


**Figure 6.15:** Case - 9. Comparison of extracted energy between the Linear estimated and Cummins' model. Incident wave with low steepness (0.012). Time period (4.07$s$) lies inside the parameter estimation bandwidth (3.9s - 4.1s).

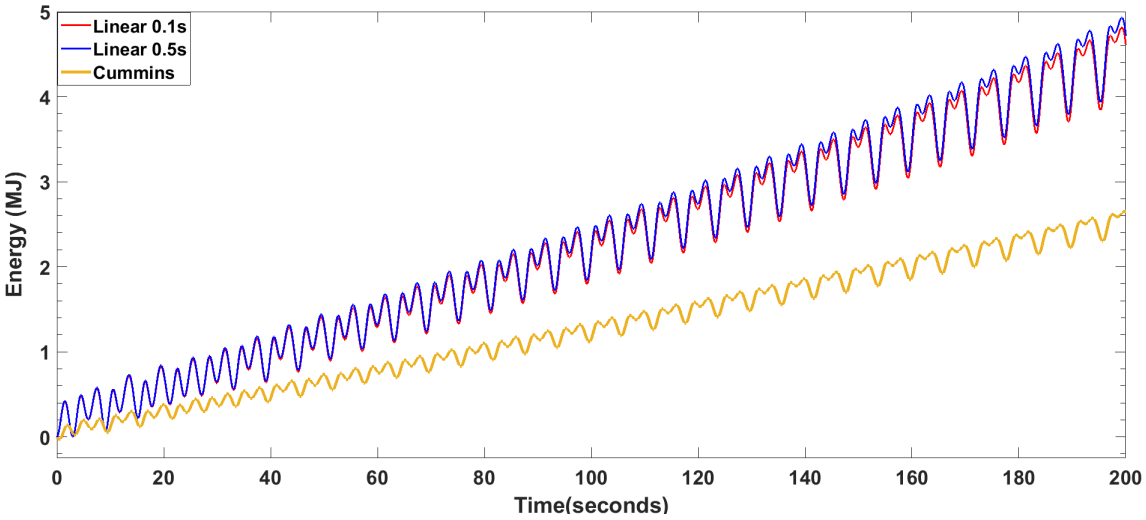


**Figure 6.16:** Case - 10. Comparison of extracted energy between the Linear estimated and Cummins' model. Incident wave with low steepness (0.012). Time period ($6s$) lies outside the parameter estimation bandwidth (3.9s - 4.1s).

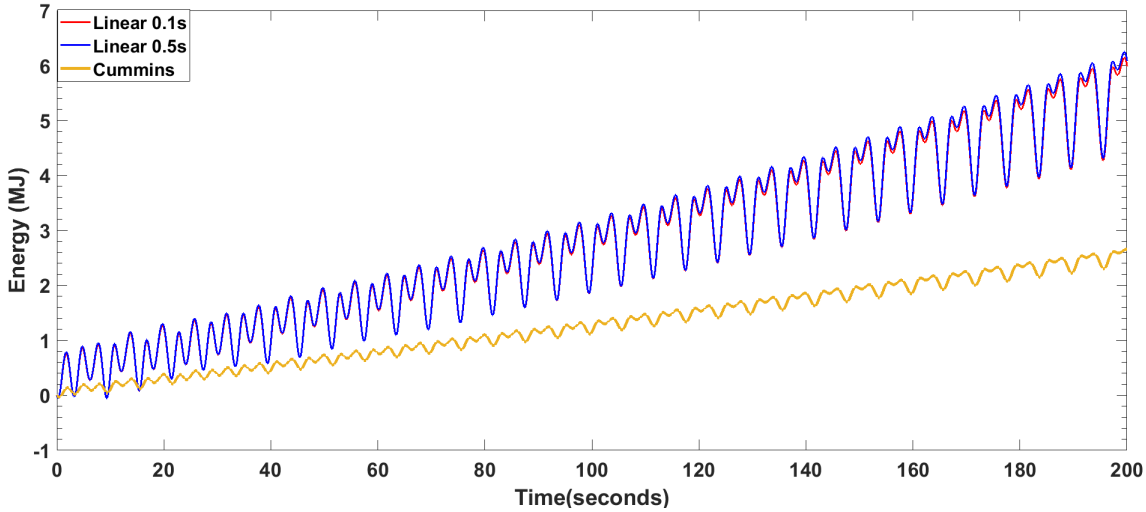


**Figure 6.17:** Case - 11. Comparison of extracted energy between the Linear estimated and Cummins' model. Incident wave with low steepness (0.012). Time period ($6s$) lies outside the parameter estimation bandwidth (7.9s - 8.1s).

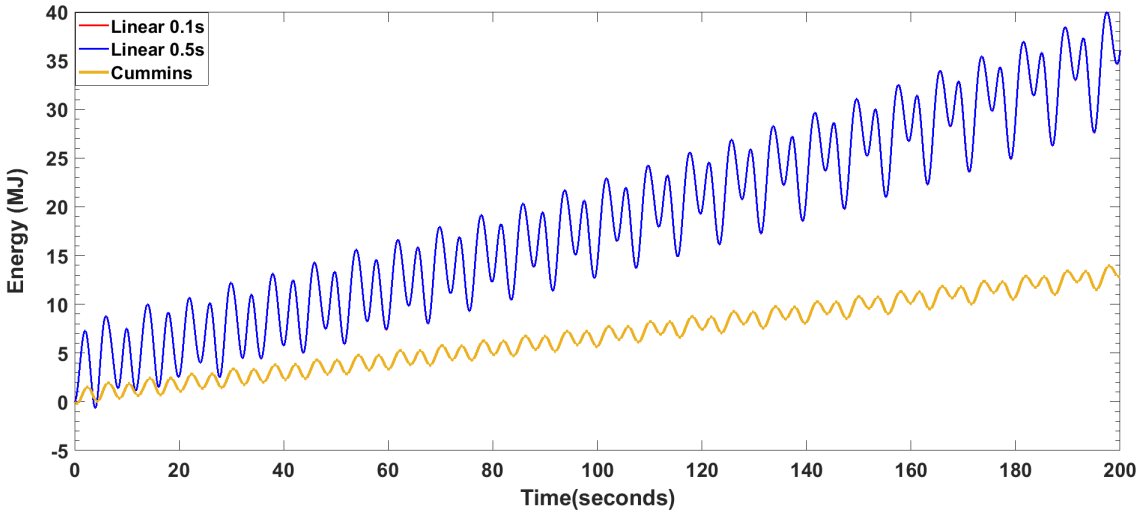


**Figure 6.18:** Case - 12. Comparison of extracted energy between the Linear estimated and Cummins' model. Incident wave with low steepness (0.018). Time period ($7.91s$) lies inside the parameter estimation bandwidth (7.9s - 8.1s).

**Table 6.2**
Extracted energy comparison at the end of 200 second time span between the linear estimated model with two bandwidths (0.1s & 0.5s) and Cummins' model.

| Case | Energy (MJ) | | |
|---|---|---|---|
| | ***Linear 0.1s*** | ***Linear 0.5s*** | ***Cummins*** |
| 5 | 1.46 | 1.42 | 0.75 |
| 6 | 12.31 | 12.66 | 6.29 |
| 7 | 18.11 | 18.74 | |
| 8 | 140.13 | 139.94 | 31.93 |
| 9 | 0.60 | 0.60 | 0.32 |
| 10 | 4.63 | 4.74 | 2.65 |
| 11 | 6.00 | 6.10 | |
| 12 | 35.92 | 35.93 | 12.89 |

Hence, it is observed that if a linear model with estimated parameters is used, then for

any combination of incident wave frequency and steepness, whether wave frequency lies inside or outside of the estimation region, the control based on the linear model gives higher extracted energy. This satisfies the second criterion stated in Chapter 5. Since, Hamiltonian based optimal control is applied to the Cummins' model, it can be said that there exists a control force that can extract higher energy from the nonlinear WEC system compared to optimal force based on the Cummins' model.

## 6.3 Effect of Estimation Frequency Bandwidth

As already stated, the frequency bandwidth used for parameter estimation plays a crucial role. It determines the number of tests required to cover the entire expected wave frequency domain. Figures (6.11), (6.12), (6.13), (6.14), (6.15), (6.16), (6.17) and (6.18) include results for two frequency bandwidths for each case. Graphically, there isn't a significant difference in energy extraction between the two, but analyzing quantitatively reveals a trend. From Table 6.2, we see that whenever the excitation frequency is outside the bandwidth, the wider band estimation model extracts higher energy compared to narrow bandwidth model and vice versa. This is a similar relationship to that observed in the un-controlled case.

## 6.4 Model Robustness to Extreme Waves or Insufficient Estimation

It is clearly established from the previous two sections and Figures (6.5), (6.6), (6.7), (6.8), (6.12, (6.13), (6.16) and 6.17) that even in regions where no parameter estimation was performed, the control based on the estimated model performed better than when based on the Cummins' model. It means the estimated linear model in general is desirable for modelling WEC hydrodynamics compared to the Cummins' model. It also means that this technique will ensure faster deployment through initial estimation, with the capability of improving the estimates by gathering data during operation.

## 6.5 Conclusion

An efficient method of modelling WECs using an estimated linear model for computing the energy optimal control solution is presented. The estimated linear model was compared against the Cummins' model for accuracy of motion during uncontrolled case. In Section 6.1, it was shown that the estimated model outperforms Cummins' model in predicting WEC motion. For all of the cases considered, the Cummins'

model had higher amplitude and phase difference compared to the linear model. It was also observed that, the narrow banded estimation was better in estimating uncontrolled WEC behavior when the estimation frequency was within the bandwidth used for estimation and vice versa. However, making the estimation bandwidth smaller came at an expense of increased number of tests to be performed to cover the entire frequency spectrum. Hence, a trade-off analysis has to be performed for a judicial choice of estimation bandwidth depending on expected sea states and ease of testing. It was also found that phase difference in displacement and velocity between the narrow $(-/+0.1s)$ and wider $(-/+0.5s)$ bandwidth linear models remained constant with the frequency of incident wave.

In this work, it was shown that a closed form energy optimal solution to the nonlinear model required satisfaction of initial conditions that were implicit in displacement and velocity. Optimal control strategy was used to show the effectiveness of the estimated model versus Cummins' model in extracting wave energy. It was shown in Section 6.2 that, optimal force from the estimated linear model resulted in higher energy extraction than optimal force from Cummins' model when applied to a nonlinear model. However, this technique facilitates the use of any control strategy in use today. Unlike other learning algorithms like Q-learning, where the learning time is similar to the duration of prevalence of a particular sea state, the proposed technique will ensure fast deployment through initial estimation, with the capability of improving the estimates by gathering data during operation. Additional analyses were performed

and it was found that the estimated model was robust to availability of insufficient estimation data and presence of random sea states.

Use of the proposed estimation technique for modelling does not rule out Cummins' model from the design process, as it may give initial estimates for buoy dimension and expected forces to build a prototype which can be used for gathering data to estimate an accurate model.

## 6.6 Future Work

This study proposed a method to increase the energy extraction of a WEC by using an estimated form of nonlinear model. The analysis was conducted to investigate the efficacy of this method for regular waves. However, for real-world implementation, it is necessary to corroborate the findings for irregular waves. It will be important to assess the accuracy of this model when parameters are estimated for the dominant frequency in the spectrum. The size of estimation bandwidth will also be a crucial factor, as it determines the number of tests to perform and is associated with the cost of operation of a WEC. Another extension that directly follows from this study is the validation of the proposed technique in a wave tank where regular waves with desired characteristics can be produced. The estimated linear model allows the application of any control strategy, but it will be important to study the variation of difference in

extracted energy between the Cummins' and the estimated model and if the model is prone to errors for specific control strategies.

# References


[1] "Climate change 2014: Synthesis report.," report, 2014.

[2] K. Gunn and C. Stock-Williams, "Quantifying the potential global market for wave power," in *Proceedings of the 4th International Conference on Ocean Engineering (ICOE 2012)*, pp. 1–7.

[3] G. Mork, S. Barstow, A. Kabuth, and M. T. Pontes, "Assessing the global wave energy potential," no. 49118, pp. 447–454, 2010. 10.1115/OMAE2010-20473.

[4] M. E. McCormick, *Ocean wave energy conversion*. Courier Corporation, 2013.

[5] *Handbook of ocean wave energy*. Ocean engineering & oceanography ; volume 7, Cham], Switzerland: Springer Open, 2017. Includes bibliographical references.

[6] D. Ross and D. Ross, *Power from the waves*. Oxford; New York: Oxford University Press, 1995.

[7] W. E. Cummins, W. T. M. B. David, and T. Symposium on Ship, *The impulse*

*response function and ship motions*. [Washington, D.C.]: Dept. of the Navy, David Taylor Model Basin, 1962.

[8] D. G. Wilson, G. Bacelli, R. G. Coe, D. L. Bull, O. Abdelkhalik, U. A. S. Korde, and R. D. Robinett III, "A comparison wec control strategies for a linear wec model," report, Sandia National Lab.(SNL-NM), Albuquerque, NM (United States), 2016.

[9] G. Giorgi and J. V. Ringwood, "Computationally efficient nonlinear froudekrylov force calculations for heaving axisymmetric wave energy point absorbers," *Journal of Ocean Engineering and Marine Energy*, vol. 3, no. 1, pp. 21–33, 2017.

[10] F. Fusco and J. V. Ringwood, "Short-term wave forecasting for real-time control of wave energy converters," *IEEE Transactions on Sustainable Energy*, vol. 1, no. 2, pp. 99–106, 2010.

[11] A. E. Bryson, *Applied optimal control : optimization, estimation, and control*. Washington: Hemisphere Pub. Corp., rev. printing. ed., 1975. Includes bibliographical references and index. (Arthur Earl).

[12] "Labman physics."

[13] U. A. Korde and J. V. Ringwood, *Hydrodynamic control of wave energy devices*.

[14] R. G. Dean, *Water wave mechanics for engineers and scientists*. Englewood Cliffs, N.J: Prentice-Hall, 1984. Includes bibliographies and indexes. (Robert George).

[15] H. E. KROGSTAD and O. A. ARNTSEN, "Linear wave theory." 2000.

[16] O. M. Faltinsen, *Hydrodynamics of high-speed marine vehicles*. Cambridge university press, 2005.

[17] H. Lamb, *Hydrodynamics*. Courier Corporation, 1945.

[18] J. Stoker, *Water Waves: The Mathematical Theory with Applications*, vol. 4. John Wiley & Sons, 1992.

[19] G. B. Whitham, *Linear and nonlinear waves*, vol. 42. John Wiley & Sons, 2011.

[20] B. Kinsman, *Wind waves: their generation and propagation on the ocean surface*. Courier Corporation, 1984.

[21] B. Datawell, "Oceanographic instruments," *Datawell Waverider Reference Manual, WR-SG, DWR-MkIII, DWR-G, Heerhugowaard, The Netherlands*, 2009.

[22] E. D. Ltd, "Wave guages," 2016.

[23] A. F. d. O. Falco, "Wave energy utilization: A review of the technologies," *Renewable and Sustainable Energy Reviews*, vol. 14, no. 3, pp. 899–918, 2010.

[24] K. Bnke and N. Ambli, "Prototype wave power stations in norway," in *Utilization of Ocean WavesWave to Energy Conversion*, pp. 34–45, ASCE.

[25] M. Ravindran and P. M. Koola, "Energy from sea wavesthe indian wave energy programme," *Current Science*, vol. 60, no. 12, pp. 676–680, 1991.

[26] A. d. O. Falco, "The shoreline owc wave power plant at the azores," in *Fourth European Wave Energy Conference, Aalborg, Denmark, Dec*, pp. 4–6.

[27] J. Falnes, "Wave-energy conversion through relative motion between two single-mode oscillating bodies," *Journal of Offshore Mechanics and Arctic Engineering*, vol. 121, no. 1, pp. 32–38, 1999.

[28] U. A. Korde, "Phase control of floating bodies from an on-board reference," *Applied Ocean Research*, vol. 23, no. 5, pp. 251–262, 2001.

[29] U. A. Korde, "Systems of reactively loaded coupled oscillating bodies in wave energy conversion," *Applied ocean research*, vol. 25, no. 2, pp. 79–91, 2003.

[30] S. J. Beatty, B. J. Buckham, and P. Wild, "Frequency response tuning for a two-body heaving wave energy converter," in *The Eighteenth International Offshore and Polar Engineering Conference*, International Society of Offshore and Polar Engineers.

[31] M. Prado, "Archimedes wave swing (aws)," *Ocean wave energy. Berlin: Springer*, pp. 297–304, 2008.

[32] S. H. Salter, "Wave power," *Nature*, vol. 249, no. 5459, pp. 720–724, 1974.

[33] S. Salter, "The swinging mace," in *Proceedings of Workshop Wave Energy R&D, Cork, Ireland*, pp. 197–206.

[34] S. Zou, O. Abdelkhalik, R. Robinett, G. Bacelli, and D. Wilson, "Optimal control of wave energy converters," *Renewable Energy*, vol. 103, pp. 217–225, 2017.

[35] O. Abdelkhalik and S. Zou, "Control of wave energy converters using a simple dynamic model," *IEEE Transactions on Sustainable Energy*, vol. 10, no. 2, pp. 579–585, 2019.

[36] S. H. Salter, J. Taylor, and N. Caldwell, "Power conversion mechanisms for wave energy," *Proceedings of the Institution of Mechanical Engineers, Part M: Journal of Engineering for the Maritime Environment*, vol. 216, no. 1, pp. 1–27, 2002.

[37] J. Taylor, "Power take-off systems: hydraulics," *Ocean wave energy. Berlin: Springer*, pp. 241–60, 2008.

[38] F. d. O. Antnio, "Modelling and control of oscillating-body wave energy converters with hydraulic power take-off and gas accumulator," *Ocean engineering*, vol. 34, no. 14-15, pp. 2021–2032, 2007.

[39] F. d. O. Antnio, "Phase control through load control of oscillating-body wave energy converters with hydraulic pto system," *Ocean Engineering*, vol. 35, no. 3-4, pp. 358–366, 2008.

[40] F. d. O. Antonio, "Wave energy utilization: A review of the technologies," *Renewable and sustainable energy reviews*, vol. 14, no. 3, pp. 899–918, 2010.

[41] K. Rhinefrank, E. Agamloh, A. von Jouanne, A. Wallace, J. Prudell, K. Kimble, J. Aills, E. Schmidt, P. Chan, and B. Sweeny, "Novel ocean energy permanent magnet linear generator buoy," *Renewable Energy*, vol. 31, no. 9, pp. 1279–1298, 2006.

[42] M. Mueller, "Electrical generators for direct drive wave energy converters," 2002.

[43] O. Danielsson, M. Leijon, K. Thorburn, M. Eriksson, and H. Bernhoff, "A direct drive wave energy converter: Simulations and experiments," no. 41960, pp. 797–801, 2005. 10.1115/OMAE2005-67391.

[44] L. Johanning, G. H. Smith, and J. Wolfram, "Mooring design approach for wave energy converters," *Proceedings of the Institution of Mechanical Engineers, Part M: Journal of Engineering for the Maritime Environment*, vol. 220, no. 4, pp. 159–174, 2006.

[45] J. Fitzgerald and L. Bergdahl, "Considering mooring cables for offshore wave

energy converters," in *Proc 7th European Wave Tidal Energy Conf, Porto, Portugal*.

[46] M. Penalba and J. V. Ringwood, "A review of wave-to-wire models for wave energy converters," *Energies*, vol. 9, no. 7, p. 506, 2016.

[47] J. V. Ringwood, G. Bacelli, and F. Fusco, "Energy-maximizing control of wave-energy converters: The development of control system technology to optimize their operation," *IEEE Control Systems Magazine*, vol. 34, no. 5, pp. 30–55, 2014.

[48] J. Falnes, "Optimum control of oscillation of wave-energy converters," *International Journal of Offshore and Polar Engineering*, vol. 12, no. 02, p. 9, 2002.

[49] J. Hals, J. Falnes, and T. Moan, "A comparison of selected strategies for adaptive control of wave energy converters," *Journal of Offshore Mechanics and Arctic Engineering*, vol. 133, no. 3, pp. 031101–031101–12, 2011. 10.1115/1.4002735.

[50] A. Babarit, G. Duclos, and A. H. Clment, "Comparison of latching control strategies for a heaving wave energy device in random sea," *Applied Ocean Research*, vol. 26, no. 5, pp. 227–238, 2004.

[51] J. Hals, T. Bjarte-Larsson, and J. Falnes, "Optimum reactive control and control by latching of a wave-absorbing semisubmerged heaving sphere," no. 36142, pp. 415–423, 2002. 10.1115/OMAE2002-28172.

[52] K. Budal and J. Falnes, "Interacting point absorbers with controlled motion," *Power from sea waves*, pp. 381–399, 1980.

[53] T. Bjarte-Larsson and J. Falnes, "Investigation of phase-controlled wave-power buoy," in *Proc. 6th European Wave Tidal Energy Conf*, pp. 47–50.

[54] J. Falnes and T. Bjarte-Larsson, "Theoretical and experimental investigation of wave energy conversion by a phase-controlled heaving body," *Proceedings of the Institution of Mechanical Engineers, Part M: Journal of Engineering for the Maritime Environment*, vol. 220, no. 4, pp. 175–183, 2006.

[55] T. Bjarte-Larsson and J. Falnes, "Laboratory experiment on heaving body with hydraulic power take-off and latching control," *Ocean Engineering*, vol. 33, no. 7, pp. 847–877, 2006.

[56] J. Falnes and P. M Lillebekken, *Budal's latching-controlled-buoy type wave-power plant.* 2003.

[57] M. Durand, A. Babarit, B. Pettinotti, O. Quillard, J. L. Toularastel, and A. Clment, *Experimental Validation of the Performances of the SEAREV Wave Energy Converter with Real-Time Latching Control.* 2007.

[58] A. Babarit and A. H. Clment, "Optimal latching control of a wave energy device in regular and irregular waves," *Applied Ocean Research*, vol. 28, no. 2, pp. 77–91, 2006.

[59] M. Kamensky, M. Guglielmi, and A. Formal'skii, "Optimal switching control of an absorber ocean wave energy device," in *2008 16th Mediterranean Conference on Control and Automation*, pp. 785–790.

[60] H. Lendenmann, K. Strømsem, M. Dai Pre, W. Arshad, A. Leirbukt, G. Tjensvoll, and T. Gulli, "Direct generation wave energy converters for optimized electrical power production," in *Proceedings of 7th European Wave Tidal Energy Conference*, 2007.

[61] D. Valerio, P. Beirao, M. J. G. C. Mendes, and J. S. d. Costa, "Comparison of control strategies performance for a wave energy converter," in *2008 16th Mediterranean Conference on Control and Automation*, pp. 773–778.

[62] P. Beiro, D. Valrio, and J. S. d. Costa, "Comparison of control strategies applied to the archimedes wave swing," in *2007 European Control Conference (ECC)*, pp. 4651–4658.

[63] D. Valrio, P. Beiro, and J. S da Costa, "Optimisation of wave energy extraction with the archimedes wave swing," *Ocean Engineering*, vol. 34, no. 17, pp. 2330–2344, 2007.

[64] G. Villarrubia, J. F. De Paz, P. Chamoso, and F. D. la Prieta, "Artificial neural networks used in optimization problems," *Neurocomputing*, vol. 272, pp. 10–16, 2018.

[65] K. S. Narendra and K. Parthasarathy, "Identification and control of dynamical systems using neural networks," *IEEE Transactions on Neural Networks*, vol. 1, no. 1, pp. 4–27, 1990.

[66] S. R. Chu, R. Shoureshi, and M. Tenorio, "Neural networks for system identification," *IEEE Control Systems Magazine*, vol. 10, no. 3, pp. 31–35, 1990.

[67] S. Giorgi, J. Davidson, and J. V. Ringwood, "Identification of wave energy device models from numerical wave tank datapart 2: Data-based model determination," *IEEE Transactions on Sustainable Energy*, vol. 7, no. 3, pp. 1020–1027, 2016.

[68] D. Valrio, M. J. G. C. Mendes, P. Beiro, and J. S da Costa, "Identification and control of the aws using neural network models," *Applied Ocean Research*, vol. 30, no. 3, pp. 178–188, 2008.

[69] S. Li and Y. Liu, *Parameter Identification Approach to Vibration Loads Based on Regularizing Neural Networks*, vol. 6. 2006.

[70] T. A. Tutunji, "Parametric system identification using neural networks," *Applied Soft Computing*, vol. 47, pp. 251–261, 2016.

[71] E. Anderlini, D. I. M. Forehand, E. Bannon, and M. Abusara, "Reactive control of a wave energy converter using artificial neural networks," *International Journal of Marine Energy*, vol. 19, pp. 207–220, 2017.

[72] A. Liaqat, M. Fukuhara, and T. Takeda, "Optimal estimation of parameters of dynamical systems by neural network collocation method," *Computer Physics Communications*, vol. 150, no. 3, pp. 215–234, 2003.

[73] R. G. Coe, G. Bacelli, D. G. Wilson, O. Abdelkhalik, U. A. Korde, and R. D. Robinett Iii, "A comparison of control strategies for wave energy converters," *International Journal of Marine Energy*, vol. 20, pp. 45–63, 2017.

[74] M. Morari and J. H. Lee, "Model predictive control: past, present and future," *Computers & Chemical Engineering*, vol. 23, no. 4, pp. 667–682, 1999.

[75] G. Li and M. R. Belmont, "Model predictive control of sea wave energy converters part i: A convex approach for the case of a single device," *Renewable Energy*, vol. 69, pp. 453–463, 2014.

[76] J. A. M. Cretel, G. Lightbody, G. P. Thomas, and A. W. Lewis, "Maximisation of energy capture by a wave-energy point absorber using model predictive control," *IFAC Proceedings Volumes*, vol. 44, no. 1, pp. 3714–3721, 2011.

[77] J. Hals, J. Falnes, and T. Moan, "Constrained optimal control of a heaving buoy wave-energy converter," *Journal of Offshore Mechanics and Arctic Engineering*, vol. 133, no. 1, pp. 011401–011401–15, 2010. 10.1115/1.4001431.

[78] S. Bellew, T. Stallard, and P. Stansby, "Optimisation of a heterogeneous array of heaving bodies," in *Proceedings of the 8th European Wave and Tidal Energy Conference*, pp. 519–527, 2009.

[79] T. K. A. Brekken, "On model predictive control for a point absorber wave energy converter," in *2011 IEEE Trondheim PowerTech*, pp. 1–8.

[80] P. Nebel, "Maximizing the efficiency of wave-energy plant using complex-conjugate control," *Proceedings of the Institution of Mechanical Engineers, Part I: Journal of Systems and Control Engineering*, vol. 206, no. 4, pp. 225–236, 1992.

[81] E. Tedeschi, M. Molinas, M. Carraro, and P. Mattavelli, "Analysis of power extraction from irregular waves by all-electric power take off," in *2010 IEEE Energy Conversion Congress and Exposition*, pp. 2370–2377.

[82] E. Tedeschi, M. Carraro, M. Molinas, and P. Mattavelli, "Effect of control strategies and power take-off efficiency on the power capture from sea waves," *IEEE Transactions on Energy Conversion*, vol. 26, no. 4, pp. 1088–1098, 2011.

[83] F. Fusco, J.-C. Gilloteaux, and J. Ringwood, "A study on prediction requirements in time-domain control of wave energy converters," *IFAC Proceedings Volumes*, vol. 43, no. 20, pp. 372–377, 2010.

[84] F. Fusco and J. Ringwood, *A Model for the Sensitivity of Non-Causal Control of Wave Energy Converters to Wave Excitation Force Prediction Errors*. 2019.

[85] F. Fusco and J. Ringwood, "Quantification of the prediction requirements in reactive control of wave energy converters," *IFAC Proceedings Volumes*, vol. 44, no. 1, pp. 11483–11488, 2011.

[86] F. Fusco and J. V. Ringwood, "A study of the prediction requirements in real-time control of wave energy converters," *IEEE Transactions on Sustainable Energy*, vol. 3, no. 1, pp. 176–184, 2012.

[87] B. Li, D. Macpherson, and J. Shek, "Direct drive wave energy converter control in irregular waves," 2011.

[88] M. P. Schoen, J. Hals, and T. Moan, "Wave prediction and fuzzy logic control of wave energy converters in irregular waves," in *2008 16th Mediterranean Conference on Control and Automation*, pp. 767–772.

[89] M. P. Schoen, J. Hals, and T. Moan, "Robust control of heaving wave energy devices in irregular waves," in *2008 16th Mediterranean Conference on Control and Automation*, pp. 779–784.

[90] M. P. Schoen, J. Hals, and T. Moan, "Wave prediction and robust control of heaving wave energy devices for irregular waves," *IEEE Transactions on Energy Conversion*, vol. 26, no. 2, pp. 627–638, 2011.

[91] H. Eidsmoen, "Optimum control of a floating wave-energy converter with restricted amplitude," *Journal of Offshore Mechanics and Arctic Engineering*, vol. 118, no. 2, pp. 96–102, 1996. 10.1115/1.2828829.

[92] E. Anderlini, D. I. M. Forehand, P. Stansell, Q. Xiao, and M. Abusara, "Control of a point absorber using reinforcement learning," *IEEE Transactions on Sustainable Energy*, vol. 7, no. 4, pp. 1681–1690, 2016.

[93] O. Abdelkhalik and S. Darani, "Optimization of nonlinear wave energy converters," *Ocean Engineering*, vol. 162, pp. 187–195, 2018.

[94] F. Fusco and J. V. Ringwood, "A simple and effective real-time controller for wave energy converters," *IEEE Transactions on Sustainable Energy*, vol. 4, no. 1, pp. 21–30, 2013.

[95] T. F. Ogilvie, "Recent progress toward the understanding and prediction of ships motion," *Proceedings of the 5th Symposium on Naval Hydrodynamics*, pp. 3–128, 1964.

[96] G. Bacelli, *Optimal control of wave energy converters*. Thesis, 2014.

[97] J. N. Newman, "Marine hydrodynamics," 1977.

[98] J. Falnes, *Ocean waves and oscillating systems : linear interactions including wave-energy extraction*. Cambridge; New York: Cambridge University Press, 2002.

[99] Z. Yu and J. Falnes, "State-space modelling of a vertical cylinder in heave," *Applied Ocean Research*, vol. 17, no. 5, pp. 265–275, 1995.

[100] R. Taghipour, T. Perez, and T. Moan, "Hybrid frequencytime domain models for dynamic response analysis of marine structures," *Ocean Engineering*, vol. 35, no. 7, pp. 685–705, 2008.

[101] K. Furuta, A. Sano, and D. P. Atherton, *State variable methods in automatic control*. Chichester [England]; New York: Wiley, 1988.

[102] C. Liu, Q. Yang, and G. Bao, "State-space approximation of convolution term in time domain analysis of a raft-type wave energy converter," *Energies*, vol. 11, no. 1, p. 169, 2018.

[103] A. Merigaud, J.-C. Gilloteaux, and J. V. Ringwood, "A nonlinear extension for linear boundary element methods in wave energy device modelling," no. 44915, pp. 615–621, 2012. 10.1115/OMAE2012-83581.

[104] M. Guerinel, A. S. Zurkinden, M. Alves, and A. J. N. A. Sarmento, "Validation of a partially nonlinear time domain model using instantaneous froude-krylov and hydrostatic forces," *10th Ewtec 2013 European Wave and Tidal Energy Conference Series*, 2013.

[105] G. Giorgi, M. Penalba, and J. Ringwood, "Nonlinear froudekrylov force representations for heaving buoy wave energy converters," in *Submitted to the 3rd Asian wave and tidal energy conference, Singapore*.

[106] T. Sarpkaya, "Force on a circular cylinder in viscous oscillatory flow at low keulegancarpenter numbers," *Journal of Fluid Mechanics*, vol. 165, pp. 61–71, 1986.

[107] D. B. Murray, "Energy storage systems for wave energy converters and microgrids," 2013.

[108] F. Wu, X. P. Zhang, and P. Ju, "Application of the battery energy storage in wave energy conversion system," in *2009 International Conference on Sustainable Power Generation and Supply*, pp. 1–4.

[109] H. Polinder, M. E. C. Damen, and F. Gardner, "Linear pm generator system for wave energy conversion in the aws," *IEEE Transactions on Energy Conversion*, vol. 19, no. 3, pp. 583–589, 2004.

[110] P. Brooking and M. Mueller, "Power conditioning of the output from a linear vernier hybrid permanent magnet generator for use in direct drive wave energy converters," 2005.

[111] B. Das and B. C. Pal, "Voltage control performance of aws connected for grid operation," *IEEE Transactions on Energy Conversion*, vol. 21, no. 2, pp. 353–361, 2006.

[112] M. Gurinel, M. Alves, and A. Sarmento, "Nonlinear modelling of the dynamics of a free floating body," *EWTEC, Southampton*, 2011.

[113] A. S. Zurkinden, F. Ferri, S. Beatty, J. P. Kofoed, and M. M. Kramer, "Non-linear numerical modeling and experimental testing of a point absorber wave energy converter," *Ocean Engineering*, vol. 78, pp. 11–21, 2014.

[114] C.-H. Lee, *WAMIT theory manual*. Cambridge, Mass.: Massachusetts Institute of Technology, Dept. of Ocean Engineering, 1995.

[115] B. S. Goh, "Necessary conditions for singular extremals in the calculus of variations," 1966.

[116] R. H. Hansen and M. M. Kramer, "Modelling and control of the wavestar prototype," *Proceedings of the 9th European Wave and Tidal Energy Conference, Ewtec 2011*, 2011.

[117] M. Atencia, E. Garca-Garaluz, H. de Arazoza, and G. Joya, "Estimation of parameters based on artificial neural networks and threshold of hiv/aids epidemic system in cuba," *Mathematical and Computer Modelling*, vol. 57, no. 11, pp. 2971–2983, 2013.

[118] A. Babarit and A. Clment, *Optimal Latching Control of a Wave Energy Device*. 2005.

[119] R. K. Pachauri, L. Mayer, and C. Intergovernmental Panel on Climate, *Climate change 2014 : synthesis report*. 2015.